JEM Journal of Experimental Medicine

ARTICLE

Clonal lineage tracing reveals mechanisms skewing CD8+ T cell fate decisions in chronic infection

Moujtaba Y. Kasmani[1,2*], Ryan Zander[2*], H. Kay Chung[3], Yao Chen[1,2], Achia Khatun[1,2], Martina Damo[4], Paytsar Topchyan[1,2], Kaitlin E. Johnson[1], Darya Levashova[5], Robert Burns[2], Ulrike M. Lorenz[5], Vera L. Tarakanova[1], Nikhil S. Joshi[4], Susan M. Kaech[3], and Weiguo Cui[1,2]

Although recent evidence demonstrates heterogeneity among CD8+ T cells during chronic infection, developmental relationships and mechanisms underlying their fate decisions remain incompletely understood. Using single-cell RNA and TCR sequencing, we traced the clonal expansion and differentiation of CD8+ T cells during chronic LCMV infection. We identified immense clonal and phenotypic diversity, including a subset termed intermediate cells. Trajectory analyses and infection models showed intermediate cells arise from progenitor cells before bifurcating into terminal effector and exhausted subsets. Genetic ablation experiments identified that type I IFN drives exhaustion through an IRF7-dependent mechanism, possibly through an IFN-stimulated subset bridging progenitor and exhausted cells. Conversely, Zeb2 was critical for generating effector cells. Intriguingly, some T cell clones exhibited lineage bias. Mechanistically, we identified that TCR avidity correlates with an exhausted fate, whereas SHP-1 selectively restricts low-avidity effector cell accumulation. Thus, our work elucidates novel mechanisms underlying CD8+ T cell fate determination during persistent infection and suggests two potential pathways leading to exhaustion.

Introduction

In settings of repeat or prolonged antigen exposure, such as chronic infection or cancer, CD8+ T cells become functionally impaired in their capacity to produce pro-inflammatory cytokines such as IFN-γ, TNF-α, and IL-2, as well as in their ability to eliminate virus-infected or cancerous cells (Zajac et al., 1998; Ahmadzadeh et al., 2009; Moskophidis et al., 1993; Wherry et al., 2003). This loss in CD8+ T cell effector function, commonly referred to as T cell "exhaustion," is accompanied by the upregulation of multiple co-inhibitory receptors, including PD-1, Tim3, Lag3, and 2B4 (Day et al., 2006; Wherry et al., 2007; Radziewicz et al., 2007; Ahmadzadeh et al., 2009). Despite their diminished function, the pool of "exhausted" CD8+ T cells still retains some cytolytic potential, as depletion of these cells results in diminished control over viral replication or tumor outgrowth (Schmitz et al., 1999; Jin et al., 1999; Johnston et al., 2014). Moreover, blockade of inhibitory molecules or their ligands, such as the PD-1–PD-L1 axis, augments the function of exhausted CD8+ T cells, thereby reinvigorating their antitumor or antiviral activity (Barber et al., 2006; Blackburn et al., 2008). Together, these observations indicate that not all exhausted CD8+ T cells are terminally dysfunctional, but rather that some are still capable of conferring a critical level of protection. As such, it has been proposed that functional adaptation is a more appropriate term for T cell exhaustion, as CD8+ T cells may continuously adjust their differentiation states to better meet the needs of a chronic infection or cancer: keeping viral levels low or limiting tumorigenesis, all while minimizing tissue damage (Utzschneider et al., 2013; Speiser et al., 2014). We speculate that one way for such a system to operate is by forming multiple distinct subsets of CD8+ T cells, with each specializing in a different function.

Supporting this idea, previous research indicates that exhausted CD8+ T cells can exist in two distinct transcriptional states during chronic viral infection, with differential expression of the transcription factors (TFs) T-bet and Eomes coordinating this cell fate decision process (Paley et al., 2012). Moreover,

[1]Department of Microbiology and Immunology, Medical College of Wisconsin, Milwaukee, WI; [2]Blood Research Institute, Versiti Wisconsin, Milwaukee, WI; [3]NOMIS Center for Immunobiology and Microbial Pathogenesis, Salk Institute for Biological Studies, La Jolla, CA; [4]Department of Immunobiology, Yale University School of Medicine, New Haven, CT; [5]Department of Microbiology, Immunology, and Cancer Biology, and Carter Immunology Center, University of Virginia, Charlottesville, VA.

*M.Y. Kasmani and R. Zander contributed equally to this paper. Correspondence to Weiguo Cui: weiguo.cui@northwestern.edu; Susan M. Kaech: skaech@salk.edu

Weiguo Cui's current address is Department of Pathology, Northwestern University, Feinberg School of Medicine, Chicago, IL.

several studies have identified that CD8+ T cells are non-homogenous and can be compartmentalized into at least two major subsets, with a self-renewing TCF-1^{hi} subset, marked by high expression levels of CXCR5 and Ly108, serving as a Progenitor population that can give rise to a more terminally exhausted TCF-1^{lo} subset that expresses higher amounts of PD-1 and Tim3 (Leong et al., 2016; Utzschneider et al., 2016b; He et al., 2016; Im et al., 2016). Importantly, TCF-1^{hi} Progenitor CD8+ T cells are responsible for providing the proliferative burst that generates effector T cells in response to immune checkpoint blockade (Im et al., 2016), and recent studies have identified that increased frequencies of progenitor CD8+ T cells correlate with improved clinical outcome and patient survival (Miller et al., 2019; Sade-Feldman et al., 2018). Thus, an identification of the factors that impact the development, maintenance, and differentiation trajectory of progenitor CD8+ T cells will undoubtedly have important clinical implications.

Previous work has demonstrated a requirement for the TFs TCF-1, Bcl-6, and E2A in promoting the formation of progenitor CD8+ T cells, whereas the TFs ID2 and Blimp-1 potently suppress their development (Leong et al., 2016; He et al., 2016; Im et al., 2016; Utzschneider et al., 2016b; Wu et al., 2016). More recently, several groups have identified that the TF Tox, which is selectively upregulated in CD8+ T cells upon persistent exposure to antigen, transcriptionally and epigenetically programs CD8+ T cell exhaustion and simultaneously restricts an effector T cell program (Khan et al., 2019; Seo et al., 2019; Scott et al., 2019; Alfei et al., 2019; Yao et al., 2019). Intriguingly, Tox was also essential for the programing and maintenance of progenitor CD8+ T cells (Yao et al., 2019), thereby ensuring CD8+ T cell longevity during chronic infection and cancer. In addition to the aforementioned TFs, several cytokines, including IL-10, IL-21, TGF-β, and type I IFNs have been implicated in regulating CD8+ T cell differentiation during chronic infection and cancer (McLane et al., 2019; Brooks et al., 2006; Tinoco et al., 2009; Elsaesser et al., 2009; Fröhlich et al., 2009; Yi et al., 2009). In particular, type I IFN production and type I IFN–stimulated genes remain elevated during chronic viral infection and may contribute to T cell dysfunction (Wilson et al., 2013; Teijaro et al., 2013). Recent work has further identified that CD8+ T cell–intrinsic type I IFN signaling inhibits progenitor CD8+ T cell formation by constraining the TCF-1–Bcl-6 axis and impeding T cell stemness (Wu et al., 2016). Nevertheless, how sustained IFN signaling impacts the differentiation trajectory of CD8+ T cells responding to chronic viral infection remains incompletely understood. Lastly, the degree of antigen exposure may also play a major role in shaping T cell dysfunction, with an Exhausted phenotype being highly dependent on the frequency of TCR engagement, but less so on TCR binding affinity (Utzschneider et al., 2016a). Collectively, these studies have identified that CD8+ T cells in chronic infection can be broadly categorized into either progenitor or terminally differentiated T cell subsets, with antigenic and environmental signals intersecting to drive distinct transcriptional programs that underlie these respective cell fate decisions.

Expanding on these findings, using high throughput single-cell RNA sequencing (scRNA-seq) to assess the heterogeneity of exhausted CD8+ T cells, our lab and others have recently uncovered the formation of a previously unrecognized effector CD8+ T cell subset that is characterized by high expression of the chemokine receptor CX_3CR1, killer cell lectin-like receptors such as KLRG1 and KLRE1, and the TFs T-bet and Zeb2 (Zander et al., 2019; Hudson et al., 2019; Chen et al., 2019; Miller et al., 2019; Kanev et al., 2019). Importantly, we and others have further identified that this CX_3CR1^+ effector CD8+ T cell subset develops in a CD4+ T cell–dependent manner, displays potent cytolytic function, is epigenetically distinct from progenitor and exhausted cells, and is critically required for control over chronic viral infection (Kanev et al., 2019; Zander et al., 2019; Hudson et al., 2019; Beltra et al., 2020; Chen et al., 2021). Notably, similar populations of effector CD8+ T cells have also been observed among tumor-infiltrating lymphocytes (TILs) and correlate with positive clinical outcomes (Yan et al., 2018).

Despite these recent advances in our understanding of the transcriptional and functional heterogeneity of CD8+ T cell responses during chronic infection and cancer, the CD8+ T cell–intrinsic and –extrinsic factors underlying these diverse developmental pathways remains incompletely understood. Moreover, although our previous work indicates that self-renewing progenitor CD8+ T cells may give rise to either PD-1^{hi} exhausted cells or CX_3CR1^+ effector cells upon recall, possibly supporting a bifurcation model of CD8+ T cell differentiation (Zander et al., 2019), the precise lineage relationship between these respective CD8+ T cell subsets, and the cellular and molecular factors that govern the fate commitment of progenitor CD8+ T cells remains unclear. Furthermore, alternative models of CD8+ T cell differentiation during chronic infection have recently been proposed, such as that of a linear differentiation trajectory (Beltra et al., 2020). Given recent advances in technology that allow for the tracking of individual T cell clones, in this study we used a paired scRNA-seq and single-cell TCR sequencing (scTCR-seq) approach to trace the clonal expansion, differentiation trajectory, and lineage commitment of virus-specific CD8+ T cells that arose naturally from an endogenous T cell repertoire, thus helping to distinguish between the aforementioned differentiation models. Additionally, using computational methods such as trajectory analysis and protein homology modeling, as well as signaling manipulation and genetic deletion experiments informed by our bioinformatic analyses, we sought to investigate how environmental signals and inherent properties of CD8+ T cells, including TCR structure and downstream signaling components, function to influence CD8+ T cell differentiation during chronic viral infection.

Results

scTCR-seq reveals clonal heterogeneity among CD8+ T cells responding to chronic viral infection

In order to dissect the clonal landscape and ultimately trace clonal evolution of the CD8+ T cell population during the late stage of chronic infection, we performed scTCR-seq alongside scRNA-seq on splenic GP33-specific CD8+ T cells isolated from three individual mice 33, 33, and 35 d after lymphocytic choriomeningitis virus (LCMV) Clone 13 infection, respectively (Fig. 1 A). We defined a clone as a group of T cells sharing the

same nucleotide sequence from the CDR3 regions of both the α and β chains of the TCR. In order to guard against errors produced by FACS sorting or sequencing misreads, we restricted our analysis to clones with at least two cells sharing the same TCR α and β chain CDR3 nucleotide sequences. This resulted in a total of 351 clones consisting of 3,386 cells among our samples.

We visualized TCR CDR3 overlap using Venn diagrams (Fig. 1 B). Intriguingly, we found that although there were a few instances of TCR CDR3 overlap among mice (M1, M2, M3) when considering either α or β chain CDR3 nucleotide sequences individually, there was no clonal overlap when α and β chain CDR3 sequences were paired on a per cell basis. This lack of overlap extended to all cells in the dataset, not only those belonging to clones with at least two cells (data not shown). A lack of clonal overlap among three genetically identical organisms speaks to the enormous diversity of the T cell repertoire, which has been estimated to range from 10^{15} to 10^{20} possible TCRs (Davis and Bjorkman, 1988; Lieber, 1991). Examining the 50 largest clones from each mouse revealed different patterns of clonal composition and dominance. Sample M3 had a single dominant clone consisting of ∼37% of all cells in the dataset. Conversely, samples M1 and M2 had slightly more evenly distributed clonal landscapes but still had some larger clones that predominated the LCMV GP33 epitope-specific CD8⁺ T cell pool (Fig. 1 C). These patterns of clonal dominance could also be seen in the TCR variable (V) and joining (J) chain gene pairings of each mouse, visualized using chord diagrams. Broader bands of V-J pairings were seen in M3 and narrower bands of V-J pairings were present in M1 and M2 (Fig. 1 D). Although the degree of heterogeneity varied among individual mice, TCR α chains were consistently more diverse than β chains (Fig. 1 D). scTCR-seq thus revealed that CD8⁺ T cells in chronic LCMV infection are highly heterogeneous in terms of TCR composition, both within individual samples and among the samples, which had no pairwise clonal overlap.

scRNA-seq defines a unique transcriptional state that may represent transitioning CD8⁺ T cells during chronic viral infection

To investigate the phenotypes of the cells in our dataset, we utilized the Seurat package in the R programming language (Butler et al., 2018; Stuart et al., 2019). The three samples previously used for scTCR-seq were supplemented with an additional pooled sample collected on day 28 post-LCMV Clone 13 infection (M4) for increased accuracy. This pooled sample acted as a single biological replicate and was generated in a separate laboratory at a different institution, helping ensure the generalizability and reproducibility of our findings. The 4,098 cells in the scRNA-seq data were visualized using Uniform Manifold Approximation and Projection (UMAP) and formed either four or five clusters depending on the resolution selected (Fig. 2 A and Fig. S1 A). We first confirmed the presence of the three major clusters that we and others have previously reported (Zander et al., 2019; Miller et al., 2019; Kanev et al., 2019) based on expression of key marker genes: progenitor (*Tcf7*, encodes TCF-1; *Slamf6*, encodes Ly108), effector (*Cx3cr1*, *Zeb2*), and exhausted (*Pdcd1*, encodes PD-1; Fig. 2 B). These clusters contained 724, 1,383, and 675 cells and comprised 17.7, 33.7, and 16.4% of the cells, respectively. The fourth major cluster in the UMAP plot contained 1,155 cells, comprised 28.2% of the total cells, and expressed some genes that were highly expressed by effector cells such as *Cx3cr1* and *Klf2*, albeit at lower levels, as well as genes expressed by exhausted cells such as *Pdcd1* and *Lag3* (Fig. 2 B). As a result of its expression of both effector and exhausted genes, we termed this cluster intermediate cells. Interestingly, one minor population of 161 cells (3.9% of total cells) was identified that merged with the exhausted cluster at lower UMAP resolution (Fig. 2 A and Fig. S1 A). This cluster expressed several genes upregulated by type I IFN stimulation such as *Ifit1*, *Ifit3*, *Isg15*, *Isg20*, and *Bst2* (Fig. S1 B). We therefore referred to this cluster as IFN-stimulated cells. Although we attempted to identify this population by flow cytometry using the protein BST2, <2% of PD-1^{hi} CD8⁺ T cells were BST2⁺ (Fig. 1 C). As we would be unable to accurately identify and quantify IFN-stimulated cells by flow cytometry in any further experiments, we elected to use our lower resolution UMAP, in which the IFN-stimulated cluster is merged with the exhausted cluster, for the majority of our scRNA-seq analyses.

To more accurately quantify the gene expression patterns of the intermediate cluster, we used Seurat's module score feature to score each cluster based on its per cell expression of the top 100 differentially expressed genes from published data of the progenitor, effector, and exhausted clusters in the late stage of LCMV Clone 13 infection (Zander et al., 2019; Fig. 2 C). As expected, each of these three clusters had the highest module score of its own genes. Although the intermediate cluster had a significantly higher effector gene module score compared to progenitor and exhausted cells, it also scored highly for the exhausted gene module (Fig. 2 C), hinting that that this population may serve as a waypoint to either a terminal effector or exhausted state. The intermediate cluster, like the effector and exhausted clusters, also had a significantly lower value of the progenitor module score compared to the progenitor cluster itself, indicating that intermediate cells are not quiescent like progenitor cells but instead may represent a transitioning developmental state between multipotency and terminal differentiation.

We previously demonstrated that differential expression of the chemokine receptor CX_3CR1 and signaling lymphocytic activation molecule (SLAM) family receptor Ly108 can be used to distinguish three major populations of virus-specific CD8⁺ T cells (CX_3CR1^{hi} effector, $Ly108^{hi}$ progenitor, and $CX_3CR1^{lo}Ly108^{lo}$ exhausted subsets; Zander et al., 2019). However, as both the effector and intermediate subsets coordinately express CX_3CR1 and lack Ly108 expression, use of these two markers alone largely groups these populations together. Thus, we sought to determine additional surface markers that may be useful in distinguishing effector versus intermediate populations while simultaneously allowing for the discrimination of exhausted and progenitor subsets. Notably, our scRNA-seq analyses indicated that the chemokine receptor *Cxcr6* was differentially expressed among the different CD8⁺ T cell subsets, with exhausted CD8⁺ T cells displaying highest expression of *Cxcr6*, followed by intermediate, effector, and progenitor cells, respectively (Fig. S1 D). Thus, we

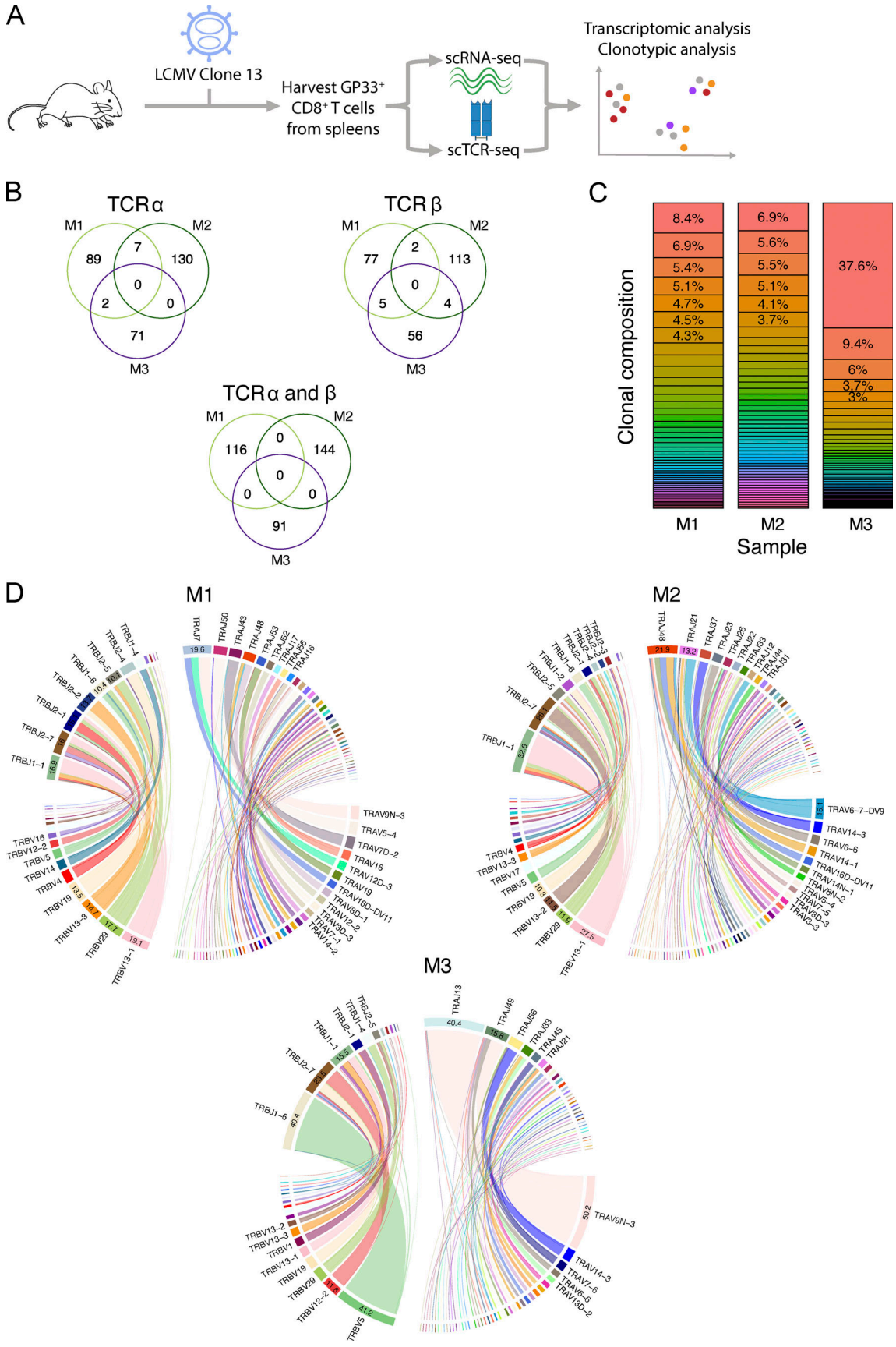

Figure 1. **scTCR-seq reveals clonal heterogeneity among LCMV GP33-specific CD8⁺ T cells. (A)** Experimental design for scRNA-seq and scTCR-seq following chronic infection with LCMV Clone 13. **(B)** Venn diagrams showing overlap among samples of CDR3 nucleotide sequences for the TCR α chain, β

chain, or paired α and β chains. **(C)** Bar plot showing percentage breakdown of the 50 largest clones per sample, each with at least two constituent cells. **(D)** Chord diagrams showing V and J gene pairings for TCR α and β chains per sample. Each band represents one unique V-J pair, with band thickness corresponding to the number of instances of that pair. For visual clarity, frequencies are only shown for TCR genes used by at least 10% of cells and gene names are only shown for TCR genes used by at least 3% of cells.

tested whether CXCR6 protein expression could be used to further stratify the CX_3CR1^+ subset into effector and intermediate populations, as recently published (Sandu et al., 2020). To do this, splenic GP33-specific $CD8^+$ T cells were co-stained for CX_3CR1, Ly108, CXCR6, and a representative set of markers (Fig. 2 D). Flow cytometry consistently distinguished the four subsets predicted by scRNA-seq: $CX_3CR1^{hi}CXCR6^{lo}$ effector, $CX_3CR1^{hi}CXCR6^{hi}$ intermediate, $CX_3CR1^{lo}Ly108^{lo}$ exhausted, and $Ly108^{hi}CX_3CR1^{lo}$ progenitor cells. Protein expression levels of key TFs and cell surface markers by the progenitor, effector, and exhausted subsets agreed with what we have previously reported: TCF-1 was highest in progenitor cells, T-bet and KLRG1 in effector cells, Tox in progenitor and exhausted cells, and Eomes and PD-1 in exhausted cells (Fig. 2, E and F). Intermediate cells did not exhibit the highest expression of any key markers, but they did express the effector markers T-bet and KLRG1 at higher levels than both progenitor and exhausted cells, indicative of an effector-like phenotype. However, intermediate cells also expressed the inhibitory receptors Tim3 and Lag3 at levels comparable to exhausted cells and significantly higher than effector cells. Despite their relatively increased expression of co-inhibitory receptors, intermediate cells displayed a similar capacity as progenitor and effector cells to degranulate and produce IFN-γ in response to peptide stimulation, whereas exhausted cells consistently displayed the lowest expression of these effector molecules following peptide stimulation (Fig. S1 E).

To better characterize the kinetics of the four subsets, in particular intermediate cells, we performed flow cytometry on $GP33^+CD8^+$ T cells at multiple time points following LCMV Clone 13 infection (Fig. S1 F). Our experiments indicated that the intermediate subset predominates during the first 2 wk of infection but that the frequencies of all subsets become more similar by the third week of infection, potentially a result of intermediate cells differentiating into terminal effector or exhausted cells. We also identified the four major $CD8^+$ T cell subsets using P14 TCR transgenic cells, and found that mean fluorescence intensity (MFI) of PD-1 is high in intermediate cells at day 15 post-infection (p.i.) but lower on day 21 p.i., whereas effector cells consistently display the lowest levels of PD-1 expression (Fig. S1, G and H). A similar distribution of progenitor, intermediate, effector, and exhausted cell subsets, as well as clear distinctions in their pattern of co-inhibitory receptor expression, was also observed among GP276- and NP396-specific CD8 T cells, suggesting that our findings on $GP33^+CD8^+$ T cells may extend to other epitope-specific T cell populations (Fig. S1, I–K). Collectively, expression of both effector and exhausted markers by intermediate cells at both the RNA and protein levels led us to hypothesize that the intermediate population serves as a branch point for progenitor cells as they transition to terminal effector or exhausted cells.

Trajectory and clonotypic analyses support the transitional nature of intermediate cells and $CD8^+$ T cell clonal multipotency

To predict differentiation trajectories, we implemented the Monocle package in R (Qiu et al., 2017). Monocle aligns cells based on gene expression levels to determine cellular differentiation in pseudotime, a term designating predicted temporal changes based on a one-time snapshot of single-cell gene expression. Our data formed a tripartite tree with a single branch point under Monocle analysis (Fig. 3 A). Within the tree structure, one branch was primarily composed of progenitor cells. As we have previously shown that these cells can give rise to the other $CD8^+$ T subsets in chronic infection (Zander et al., 2019), we designated the tip of this branch to be the start point of pseudotime (Fig. S2 A). The two other branches were designated effector and exhausted due to their respective enrichment with each of these two cell types. Intermediate cells were distributed among all three branches (32.6% progenitor branch, 51.6% effector branch, 15.6% exhausted branch; Fig. 3 A and Fig. S2 B), lending further credence to the hypothesis that they have the potential to develop into both effector and exhausted cells.

Expression of differentially expressed marker genes for the subsets changed if traversing the progenitor to effector or progenitor to exhausted branch paths across pseudotime. Effector markers, such as *Cx3cr1* and *Zeb2*, increased in the progenitor branch after an initial lull in pseudotime when progenitor cells represented most of the population. Increased expression of these genes correlated with a predominance of intermediate cells before the pseudotime branchpoint. However, expression of these genes either continued to increase or else sharply dropped off at the branchpoint depending on whether intermediate cells diverged into the effector or exhausted branch, respectively (Fig. 3 B). Exhaustion markers such as *Pdcd1*, *Lag3*, *Eomes*, and *Nr4a2* also had divergent expression upon reaching the branch point: levels of these markers in the effector branch were consistently nonzero but always stayed at lower absolute levels compared to the exhausted branch (Fig. 3 C). Interestingly, markers of type I IFN stimulation followed the same trend as established exhaustion markers but were even more sharply downregulated in intermediate cells (Fig. 3 D). Applying our higher resolution UMAP parameters (Fig. S1 A) to this analysis, we found that IFN-stimulated cells were located exclusively at the tips of the progenitor and exhausted branches (Fig. S2 C) and were responsible for driving the bimodal expression of IFN-stimulated genes in the progenitor-to-exhausted pseudotime trajectory (Fig. S2 D). This raised the possibility that the IFN-stimulated subset directly bridges progenitor and exhausted cells without having to pass through the intermediate state.

Trajectory analyses predicted differentiation patterns at the cellular level, but not at the clonal level. $CD8^+$ T cells in acute viral infection have been shown to follow a "one cell, multiple

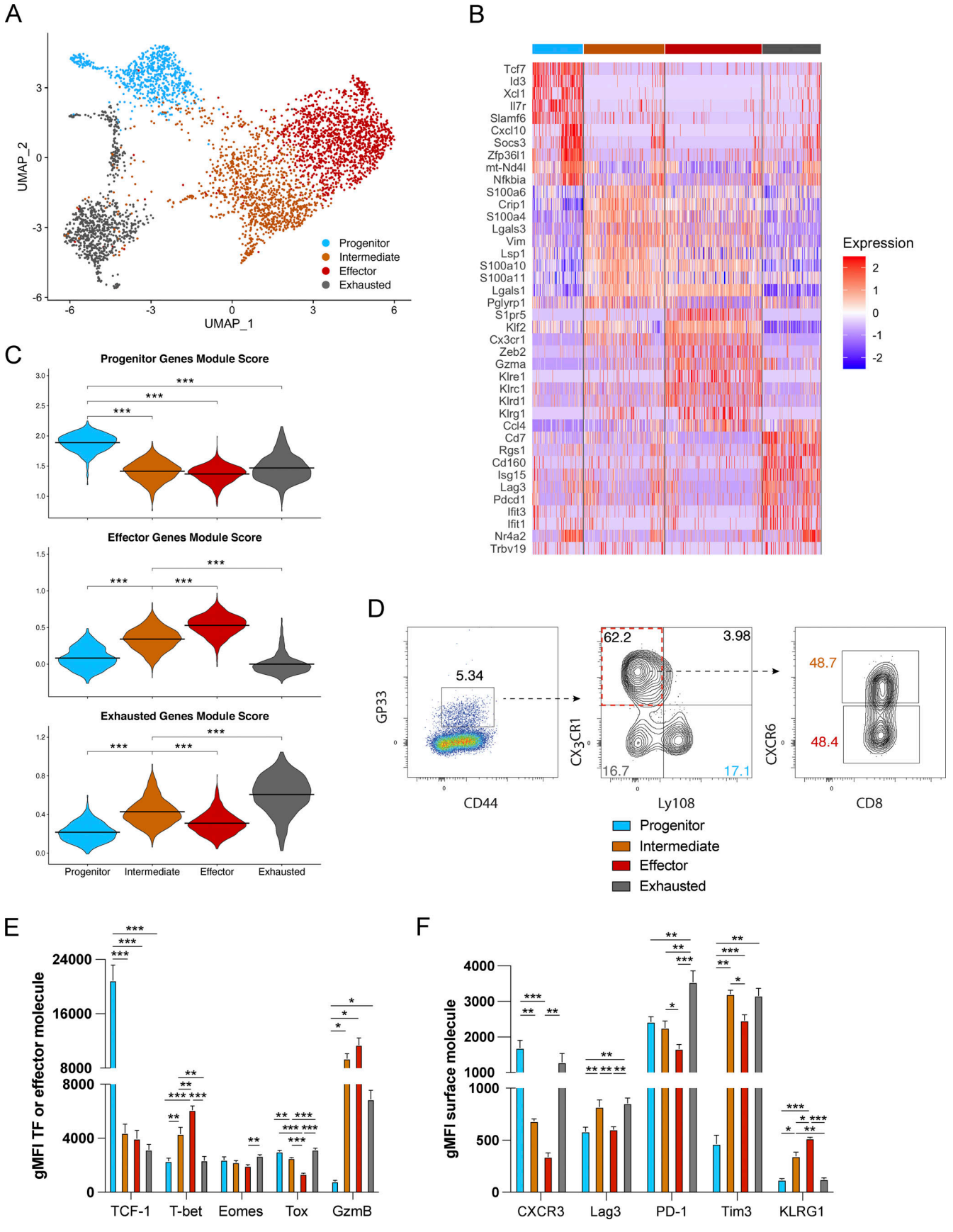

Figure 2. **scRNA-seq defines a unique transcriptional state that may represent transitioning CD8⁺ T cells during chronic viral infection. (A)** UMAP plot of splenic GP33⁺ CD8⁺ T cells from four mice on days 28, 33, 33, and 35 after LCMV Clone 13 infection. Each dot represents one cell, cells are colored by cluster

identity. **(B)** Heatmap of the top 10 differentially expressed genes per cluster. **(C)** Violin plots of module scores based on the top 100 differentially expressed genes in the progenitor, effector, and exhausted clusters as published in Zander et al. (2019). **(D)** Representative flow plots of splenic GP33$^+$CD44$^+$CD8$^+$ T cell subsets using the markers CX_3CR1, Ly108, and CXCR6. Cells were harvested on day 30 p.i. **(E)** Summary data of D showing relative expression of TFs and effector molecules among the subsets. **(F)** As in E but showing the relative expression of surface molecules. gMFI, geometric MFI. Data (mean ± SEM) in E and F are from three to six mice and are representative of at least three independent experiments. * P < 0.05, ** P < 0.01, *** P < 0.001. See also Fig. S1.

fate" model of differentiation (Gerlach et al., 2010). To investigate whether this holds true in the chronic infection setting and to trace clone lineages, we combined our scTCR-seq and scRNA-seq data. We noticed that the overwhelming majority of CD8$^+$ T cell clones were distributed among multiple clusters and not cluster restricted, including three of the largest clones (Fig. 3 E). Given that T cells with identical TCR α and β chains are logically a clone that derive from a single naive T cell ancestor, these results suggest that most naive CD8$^+$ T cells can give rise to multi-fated virus-specific CD8$^+$ T cells after activation and clonal expansion. However, some rare, small clones were restricted to a particular cluster. Specifically, 17 clones were unique to the progenitor cluster, 18 to the intermediate cluster, 49 to the effector cluster, and 27 to the exhausted cluster. In contrast, 218, 236, 200, and 223 clones had constituent cells in the progenitor, intermediate, effector, and exhausted cluster, respectively, but also had cells in at least one other cluster.

In order to specifically study clones arising from progenitor cells, we limited our analysis to clones that had some degree of membership in the progenitor cluster (progenitor-overlapping clones), thereby excluding all clones that we cannot conclusively ascertain derived from progenitor cells. As this process excluded all clones restricted to any one cluster other than the progenitor cluster, we also excluded progenitor cluster-restricted clones, which are likely to be truly quiescent, to avoid biasing the data. We then measured clonal diversity through the inverse Simpson diversity index (Fig. 3 F). Doing so revealed comparable clonal diversity among most clusters except for the progenitor cluster, which had noticeably higher diversity than all other clusters. This observation implies that clonal diversity gradually decreases as progenitor cells undergo terminal differentiation, in line with studies that have shown a decrease in CD8$^+$ T cell clonal diversity during chronic simian immunodeficiency virus infection and chronic human CMV infection (Sircar et al., 2010; Schober et al., 2020), as well as a recent study showing a narrowing of the GP33-specific CD8$^+$ T cell repertoire over the course of chronic LCMV infection (Chang et al., 2020).

We then used the R package STARTRAC (Zhang et al., 2018) to analyze the spread of individual clones among the four clusters. The STARTRAC Expansion Index provided an independent confirmation of our analysis of diversity, as the progenitor cluster had the lowest index and thus the highest diversity (Fig. S2 E). The STARTRAC Transition Index, which measures the potential of differentiation to another phenotype, had opposite values, with the intermediate cluster scoring the highest and the progenitor cluster the lowest (Fig. S2 F). Intercluster transition potential was also analyzed more granularly using the Pairwise STARTRAC Transition Index (Fig. 2 G). This metric showed that the intermediate cluster exhibited equal transition potential with the effector cluster (0.69) and the exhausted cluster (0.69). In short, these data suggest that the progenitor cluster is more quiescent and stem-like, as has previously been observed (Im et al., 2016), whereas the intermediate cells that derive from it are more active in transitioning into terminally differentiated effector or exhausted cells.

Adoptive transfer of intermediate cells validates their multipotency

Collectively, trajectory analysis and clonotypic analysis of our scRNA-seq and scTCR-seq data suggested that intermediate cells are capable of generating both effector and exhausted cells. To validate this in vivo, we performed adoptive transfer experiments in which progenitor (Ly108^{hi}CX_3CR1^{lo}), intermediate (CX_3CR1^{hi}CXCR6^{hi}), effector (CX_3CR1^{hi}CXCR6^{lo}), and exhausted (CX_3CR1^{lo}Ly108^{lo}PD-1^{hi}) CD8$^+$ T cells from LCMV Clone 13–infected mice were sort-purified and adoptively transferred into congenically marked infection-matched recipient mice (Fig. 4 A). Consistent with their exhausted phenotype (Fig. 2 B, E and F; Zander et al., 2019), CX^3CR1^{lo}Ly108^{lo} CD8$^+$ T cells accumulated to the lowest extent compared to progenitor, intermediate, and effector cells (Fig. 4, B and C). Importantly, 8 d after transfer, both exhausted and effector donor-derived cells largely retained their original phenotype (Fig. 4, B and D), further indicating that these populations have reached a terminal stage of differentiation. By contrast, while ∼50% of progenitor cells appeared to maintain their quiescence and retained high expression of Ly108, the other half displayed an inherent competency to give rise to intermediate, effector, and exhausted cell subsets, further supporting their stem-like properties (Fig. 4, B and D). Strikingly, and in corroboration with our trajectory and clonotypic analyses, a large proportion of intermediate donor-derived cells acquired either an effector (∼40%) or exhausted (∼30%) phenotype, respectively (Fig. 4, B and D), thereby validating the transitional nature of this intermediate population. Of note, although only a small proportion of intermediate cells was recovered from progenitor donor cells (<5% versus ∼15% effector and ∼40% exhausted), we speculate that this is likely due to the transitional nature of the intermediate subset (Fig. 4, B and D), with this population rapidly converting to a terminally differentiated effector or exhausted state in a rather short time frame. Taken together, these data indicate that during persistent viral infection, a large fraction of progenitor CD8$^+$ T cells may develop into a transitory intermediate population that also displays a degree of multipotency before committing to a more terminal effector or exhausted cell fate.

The transcription factors IRF7 and Zeb2 intrinsically drive CD8$^+$ T cell differentiation toward exhausted and effector fates, respectively

Previous work has shown that inhibiting type I IFN signaling by blocking the type I IFN receptor IFNAR leads to an increase in

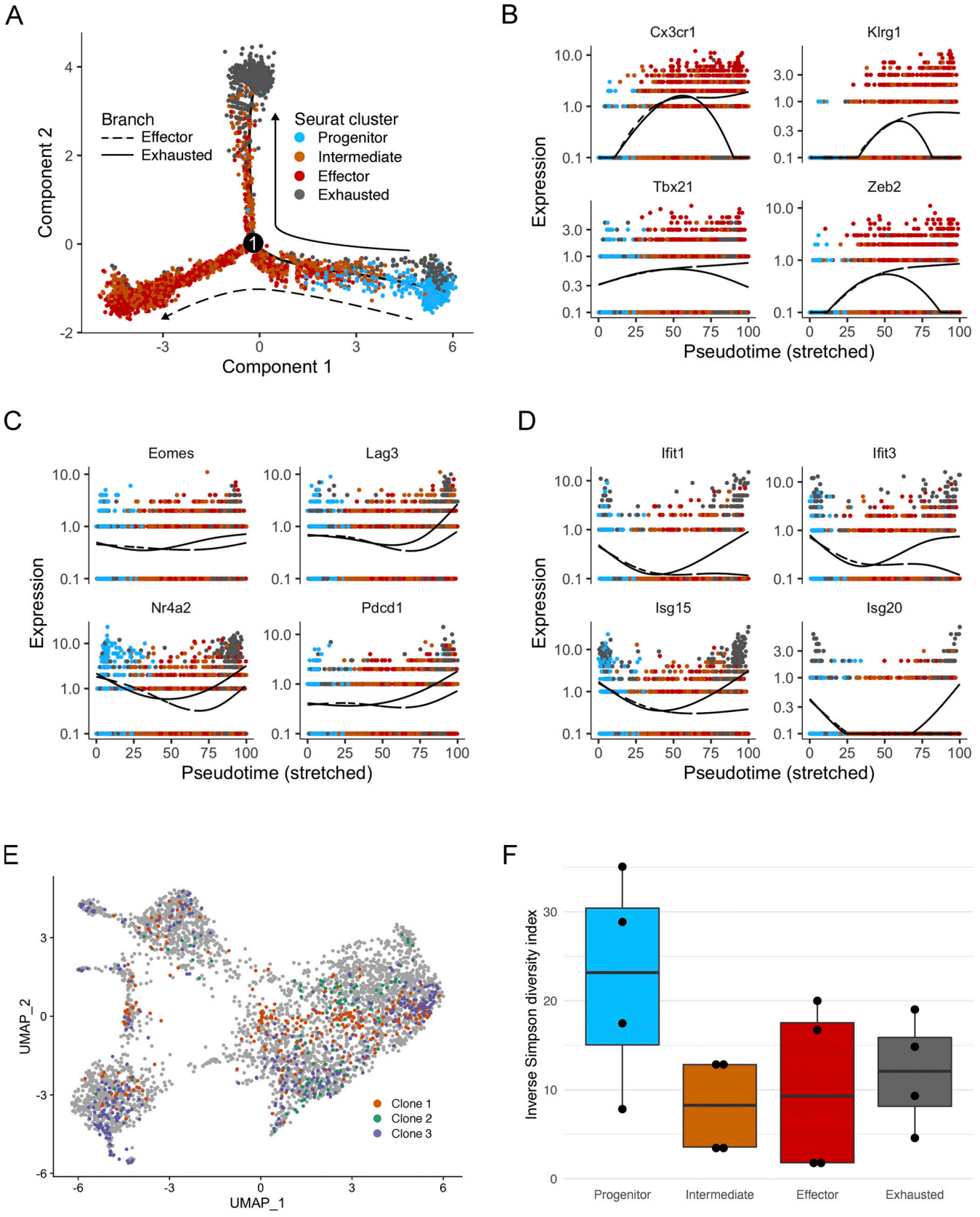

Figure 3. **Trajectory and clonotypic analyses support the transitional nature of intermediate cells and CD8⁺ T cell clonal multipotency. (A)** Monocle tree trajectory plot showing predicted cellular differentiation based on trajectory analysis. Cells are colored by Seurat cluster. **(B–D)** Plots showing effector (B), exhausted (C), and IFN-stimulated (D) gene expression over pseudotime. Dashed and solid lines denote transition from the progenitor to the effector or exhausted Monocle state, respectively. Colors denote the Seurat cluster identity of each cell. **(E)** UMAP plot as in Fig. 2 A but colored by clone membership.

Three representative clones shown. **(F)** Inverse Simpson diversity index calculated for clones in each cluster. Only clones with some, but not all, constituent cells in the progenitor cluster were included. Higher values indicate more clonal diversity. See also Fig. S2.

TCF-1^{hi} CD8$^+$ T cells during chronic infection (Huang et al., 2019; Wu et al., 2016). Moreover, TCR transgenic IFNAR$^{-/-}$ P14 cells, which recognize the GP33 epitope of LCMV, maintain higher amounts of TCF-1 expression compared to WT P14 cells, suggesting that CD8$^+$ T cell–intrinsic IFNAR signaling may promote terminal differentiation (Wu et al., 2016). However, these studies were conducted before data on the existence of intermediate and effector cells were available. Thus, whether type I IFNs regulate the bifurcation of progenitor cells toward an effector versus an exhausted fate through the intermediate population has hitherto remained unclear.

In order to obtain a preliminary intuition for the role of IFN signaling in CD8$^+$ T cell differentiation during chronic viral infection, we generated a module score based on the Gene Set Enrichment Analysis (GSEA) Reactome pathway "Interferon Signaling" (GSEA systematic name M983). A violin plot of this module score showed enrichment for IFN signaling in progenitor, intermediate, and exhausted cells, with effector cells exhibiting a significantly lower score than all three other clusters (Fig. S3 A). This analysis, along with differential expression of IFN-stimulated genes like *Ifit1* and *Isg15* in IFN-stimulated or exhausted cells (Figs. 2 B, 3 D, and Fig. S1 B) and existing data in the literature, suggests that type I IFN signaling selectively drives progenitor cells to differentiate into exhausted cells. To test this hypothesis, we treated mice with Poly (I:C), a synthetic analogue of double-stranded RNA that acts as a TLR3 agonist and a potent inducer of type I IFN production (Field et al., 1972; Ngoi et al., 2008), beginning after the second week of persistent LCMV Clone 13 infection (Fig. 5 A). We harvested spleens and peripheral blood on day 24 p.i. and performed flow cytometry, separating GP33$^+$CD44$^+$CD8$^+$ T cells by CX$_3$CR1, Ly108, and CXCR6 expression to detect the four subsets (Fig. 5 B and Fig. S3 B). Compared to the control group, mice administered Poly (I:C) displayed a trend but non-significant decrease in the percentage of splenic GP33-specific CD8$^+$ T cells (Fig. S3 C). Notably, however, Poly (I:C)–treated mice had significantly higher proportions of exhausted cells and lower proportions of progenitor, intermediate, and effector cells (Fig. 5 C). These alterations in the subset distribution of CD8$^+$ T cells were further accompanied by a significant decrease in the number of progenitor, intermediate, and effector cells in mice treated with Poly (I:C), although the number of exhausted cells was comparable to control mice (Fig. S3 D). Strikingly, we further observed over a fivefold decrease in the proportion of circulating progenitor CD8$^+$ T cells in Poly (I:C)–treated mice (Fig. S3 E), consistent with a role for type I IFNs in limiting progenitor cell formation or maintenance. Of note, this decrease in progenitor cells found in the blood was accompanied by a significant increase in the proportion of effector, but not exhausted, CD8$^+$ T cells detected in the circulation, likely as a result of exhausted CD8$^+$ T cells being largely absent from the blood (Zander et al., 2019; Beltra et al., 2020). Together, these data support our hypothesis by showing that progenitor CD8$^+$ T cell differentiation is diverted away from an effector fate and driven toward an exhausted phenotype in the presence of strong, persistent type I IFN signaling. Furthermore, the ratio of expression of the effector cell–associated TF T-bet to that of the exhausted cell–associated TF Eomes was significantly lower following Poly (I:C) treatment (Fig. S3 F). To test functionality after Poly (I:C) treatment, we stimulated CD8$^+$ T cells with GP33 peptide ex vivo and observed a significant decrease in the proportion of CD107a$^+$IFNγ$^+$ antigen-specific CD8$^+$ T cells in mice given Poly (I:C) compared to control mice (Fig. S3 G). This shows that Poly (I:C) treatment impairs the functional production of inflammatory cytokines and inhibits degranulation, both of which are properties we have previously shown to be associated more with cytolytic effector cells than exhausted cells (Zander et al., 2019). Collectively, these experiments demonstrate that prolonged and increased type I IFN signaling biases progenitor cells toward developing into exhausted cells.

Notably, our scRNA-seq data showed that IFN-stimulated cells differentially expressed several interferon-stimulated genes (ISGs) such as *Ifit1*, *Ifit3*, and *Isg15* (Fig. S1 B) and may bridge progenitor and exhausted cells (Fig. S2, C and D). These results suggest that direct IFNAR signaling and downstream transcriptional regulators in CD8$^+$ T cells could be responsible for promoting progenitor CD8$^+$ T cell differentiation toward a terminal exhausted phenotype. In further support of this, the R package SCENIC, which we used to perform unbiased gene regulatory network analysis on our scRNA-seq data, predicted that the *Stat1*, *Stat2*, *Irf7*, and *Irf9* regulons (TFs and their putative downstream targets) were all activated in a small number of progenitor and exhausted cells as well almost all IFN-stimulated cells (Fig. S3 H). Together, these findings suggest that several TFs downstream of type I IFN signaling may cooperate to coordinate a transcriptional program in CD8$^+$ T cells that skews their differentiation toward exhaustion. Of particular interest was the TF IRF7, which is strongly induced by the type I IFN–activated complex ISGF3, a hetero-trimeric transcriptional activator comprised of the TFs STAT1, STAT2, and IRF9 (Honda et al., 2006). Although prior studies have identified a negligible role for CD8$^+$ T cell–intrinsic IRF7 expression in regulating CD8$^+$ T cell responses in the context of acute viral infection (Zhou et al., 2012; Li et al., 2013), we reasoned that IRF7 may play a more prominent role in the setting of persistent infection, given that type I IFN production is augmented during chronic viral infection, and ISGs remain elevated for several weeks after LCMV Cl13 infection (Teijaro et al., 2013; Wilson et al., 2013). To test this, we generated competitive mixed bone marrow (MBM) chimera mice by reconstituting lethally irradiated Ly5.1 recipient mice with bone marrow from the following donors: CD8$^{-/-}$ (70%) + Thy1.1 WT (15%) + IRF7$^{-/-}$ (15%; Fig. 5 D). Notably, this experimental design helps control for WT and IRF7$^{-/-}$ CD8$^+$ T cells experience a similar degree of exposure to both viral load and inflammation in the same host. These MBM chimera mice were then challenged with LCMV Cl13, and we proceeded to assess virus-specific CD8$^+$ T cell responses in the spleens of these

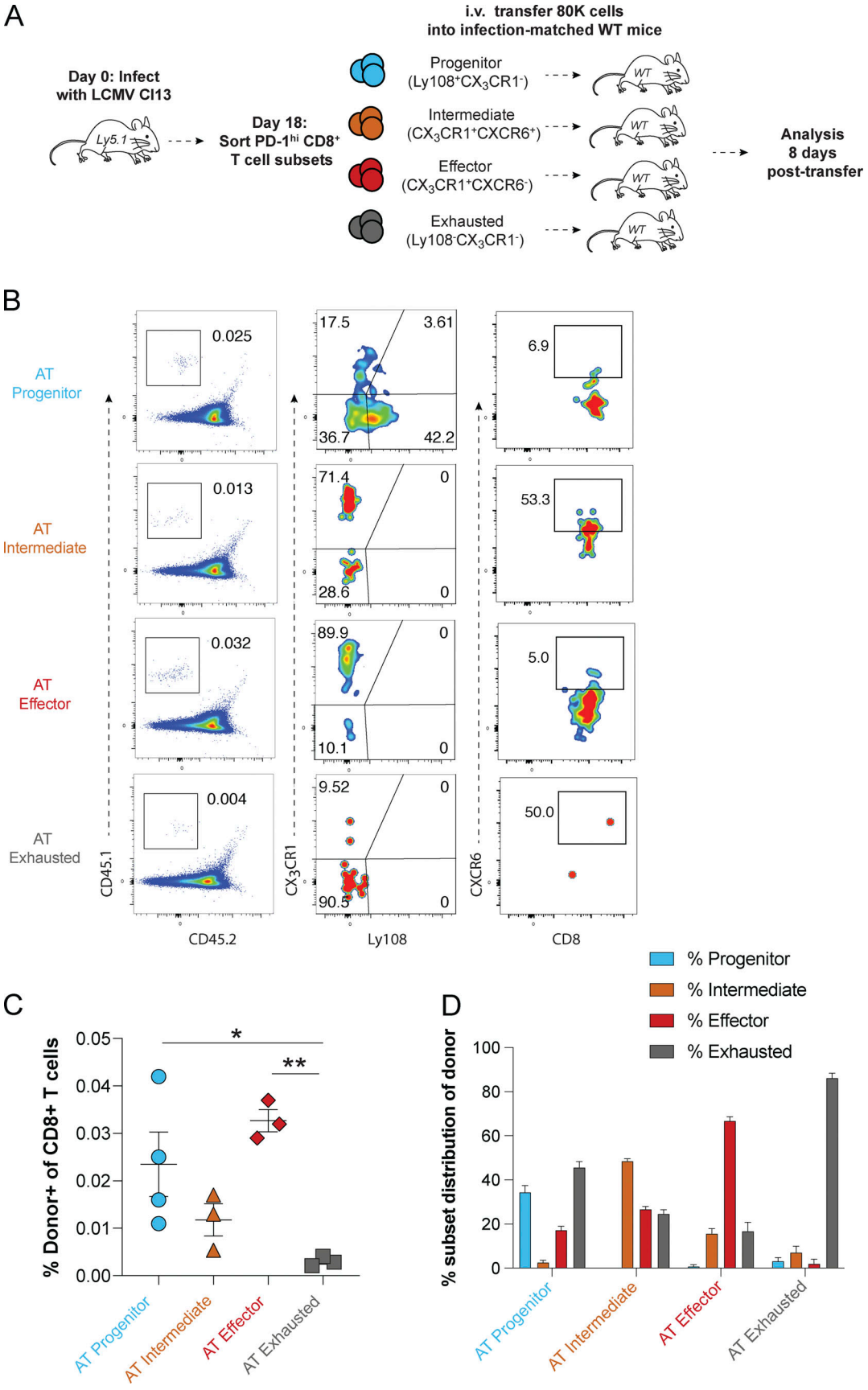

Figure 4. **The intermediate population can give rise to both effector and exhausted CD8⁺ T cells in vivo. (A)** Experimental design. **(B)** Representative flow plots showing the proportion of recovered donor cells in the spleen, and their respective phenotypes, following adoptive transfer (AT). **(C)** Summary data

showing the proportion of donor-derived cells in the spleen. **(D)** Summary data showing the percentage subset distribution of donor-derived cells at 8 d after adoptive transfer. Data (mean ± SEM) in C and D are from three to four mice per group and are representative of two independent experiments. * P < 0.05, ** P < 0.01.

experimental mice on day 18 p.i. (Fig. 5 E). Importantly, while we observed no appreciable difference between WT and IRF7$^{-/-}$ CD8$^+$ T cells in their capacity to expand or accumulate, IRF7$^{-/-}$ GP33-specific CD8$^+$ T cells displayed approximately a twofold increase in progenitor CD8$^+$ T cell formation and a striking two- to threefold decrease in the development of exhausted CD8$^+$ T cells, whereas the proportions of effector and intermediate cells did not significantly differ (Fig. 5 F). In corroboration with having a diminished frequency of exhausted T cells, IRF7$^{-/-}$ CD8$^+$ T cells displayed an increased ratio of T-bet to Eomes expression and decreased levels

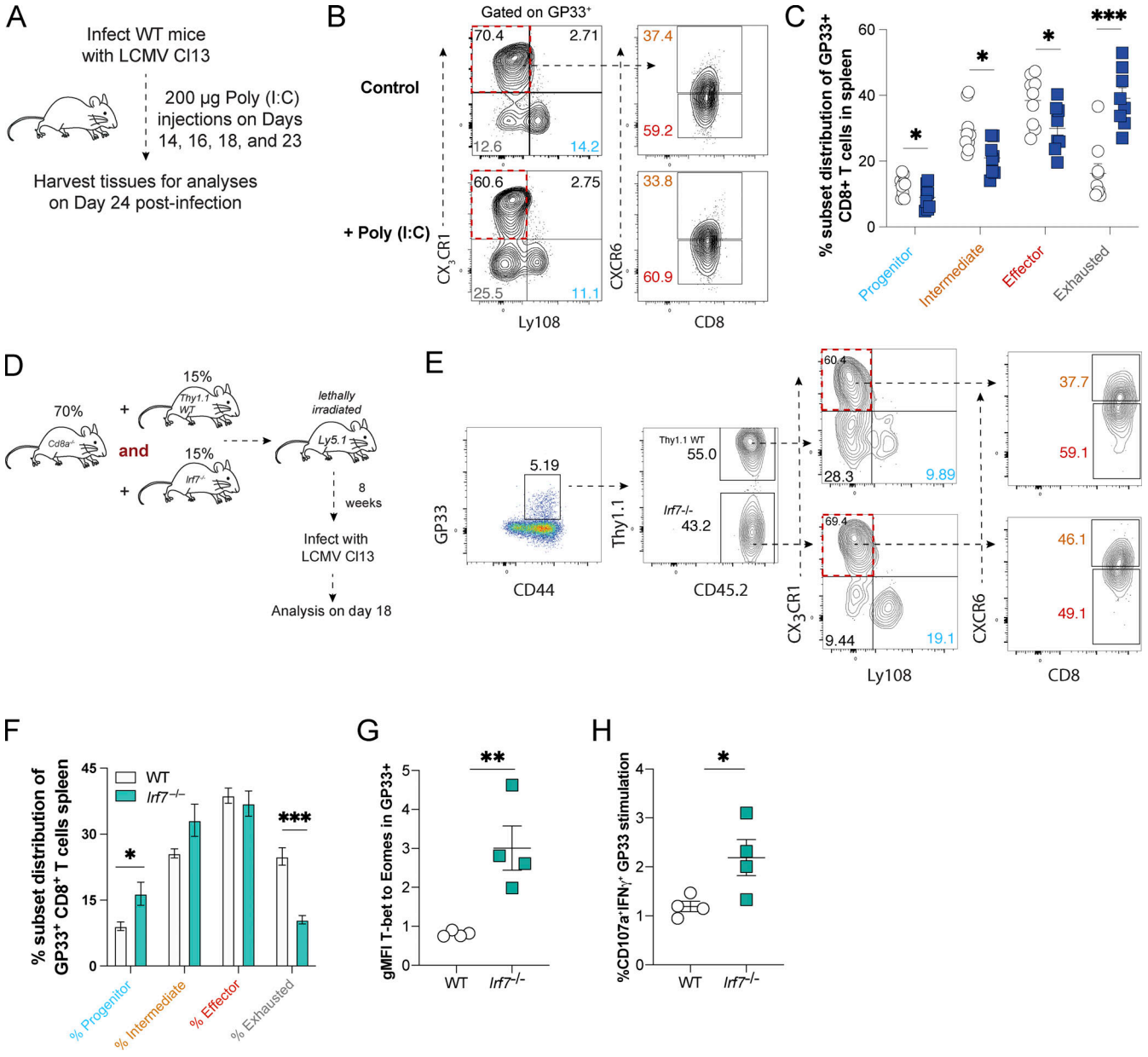

Figure 5. **Type I IFN–induced IRF7 is intrinsically required for differentiation of exhausted CD8$^+$ T cells. (A)** Experimental design for type I IFN signaling studies using Poly (I:C). **(B and C)** Representative flow plots (B) and quantified subset distribution frequencies (C) of GP33 antigen-specific CD8$^+$ T cells in the spleens of control mice or mice given Poly (I:C). **(D)** Experimental design for IRF7$^{-/-}$ MBM chimera experiments. **(E and F)** Representative flow plots (E) and summary data (F) showing the subset distribution of WT and IRF7$^{-/-}$ CD8 T cells. **(G)** Summary depicting the ratio in geometric MFI (gMFI) of T-bet to Eomes in WT and IRF7$^{-/-}$ GP33-specific CD8$^+$ T cells. **(H)** Frequency of CD107a$^+$ IFNγ$^+$ CD8$^+$ T cells upon ex vivo stimulation with GP33 peptide. Data (mean ± SEM) in B and C are from three to four mice per group and are pooled from two independent experiments. Data (mean ± SEM) in E–H are from four mice per group and are representative of two independent experiments. * P < 0.05, ** P < 0.01, *** P < 0.001. See also Fig. S3.

of Tim3 and 2B4 relative to their WT counterparts (Fig. 5 G and Fig. S3 I). These alterations were further associated with IRF7$^{-/-}$ CD8$^+$ T cells displaying an augmented capacity to degranulate and produce IFN-γ upon ex vivo peptide stimulation (Fig. 5 H). Collectively, these results indicate that CD8$^+$ T cell–intrinsic IRF7 expression drives progenitor CD8$^+$ T cell differentiation toward an exhausted state during chronic viral infection. Thus, these findings elucidated a TF directly downstream of type I IFN signaling that contributes to CD8$^+$ T cell dysfunction during persistent viral infection.

As IRF7 was capable of selectively driving an exhausted fate, we wondered whether there may an analogous TF that promotes a terminal effector fate. The TF Zeb2 has been shown to be critical for the generation of short-lived effector cells (SLECs) in acute viral infection (Dominguez et al., 2015). Given that SLECs and effector cells from chronic infection share certain transcriptomic and epigenetic similarities, as recently uncovered by our lab (Chen et al., 2021), we hypothesized that Zeb2 may also play a critical role in the function of effector cells in chronic viral infection. Supporting this hypothesis, we noted that *Zeb2* was enriched in effector cells (Fig. 2 B) and was predicted by Monocle pseudotime analysis to bifurcate in expression between intermediate cells that generated effector and exhausted cells (Fig. 3 B). To test our hypothesis, we first infected WT (GzB-Cre$^-$ Zeb2$^{flox/flox}$) or Zeb2 cKO (GzB-Cre$^+$ Zeb2$^{flox/flox}$) mice with LCMV Clone 13 and harvested spleens on day 30 p.i. (Fig. 6 A). Upon analyzing PD-1$^+$ CD8$^+$ T cells specific for either GP33 or GP276, we found a significant reduction in the frequency of both intermediate and effector cells. We also observed 1.5- to twofold increases in the frequency of both progenitor and exhausted cells that approached statistical significance (Fig. 6 B). To validate these findings in a more specific system, we performed an experiment in which 20,000 Zeb2$^{+/+}$ (GzB-Cre$^-$ Zeb2$^{flox/flox}$) or Zeb2$^{-/-}$ (GzB-Cre$^+$ Zeb2$^{flox/flox}$) Ly5.1 P14 TCR transgenic CD8$^+$ T cells were adoptively transferred into WT C57BL/6 mice 1 d before LCMV Clone 13 infection. Then on day 18 p.i., the mice were sacrificed and spleens were harvested (Fig. 6 C). Ablation of Zeb2 in a CD8$^+$ T cell–intrinsic manner led to a three- to fourfold decrease in the frequency of both intermediate and effector P14 cells. Conversely, there was a significant increase in the frequency of both progenitor and exhausted P14 cells (Fig. 6 D). These data indicate that the TF Zeb2 is intrinsically required for intermediate and effector CD8$^+$ T cell formation by promoting both progenitor to intermediate and intermediate to effector transitions, thus helping to divert intermediate cells from a terminal exhausted cell fate.

TCR:peptide MHC (pMHC) quantitative avidity correlates with phenotypic skewing of CD8$^+$ T cell clones

To further investigate how various signaling pathways impact CD8$^+$ T cell fate during chronic viral infection, we turned to studying the TCR. TCR structure, affinity, and avidity for pMHC have been documented to play important roles in clonal competition and phenotypic differentiation of CD8$^+$ T cells in different model systems (Schober et al., 2020; Trautmann et al., 2005; King et al., 2012). We thus leveraged our scTCR-seq data to investigate these phenomena in CD8$^+$ T cells during chronic LCMV infection, focusing on their impact on effector and exhausted CD8$^+$ T cell development. We began using TCRdist (Dash et al., 2017) to analyze paired α and β chain CDR3 amino acid motifs in effector-biased and exhausted-biased clones, which we defined as clones with at least 50% of constituent cells in the effector or exhausted Monocle branch, respectively. Interestingly, we found that values for CDR3 amino acid sequence length and charge, as well as two separate metrics for hydrophobicity, were comparable between effector- and exhausted-biased clones (Fig. S4 A). As CDR3 sequences are the portion of the TCR that most directly contact antigen presented on MHC, they have a large influence on TCR binding affinity for pMHC complexes (Borg et al., 2005). Thus, we investigated the relationship between the TCR:pMHC binding affinity of a CD8$^+$ T cell clone and that clone's fate decisions during chronic viral infection.

To evaluate binding affinity, we generated homology protein models from our scTCR-seq data to calculate a metric that we termed quantitative affinity (Fig. 7 A and Materials and methods). We began by investigating the link between TCR:pMHC binding affinity and the development of an exhausted phenotype, as multiple reports have linked increased antigen exposure and TCR signaling to exhaustion (Mueller and Ahmed, 2009; Richter et al., 2012; Utzschneider et al., 2016a). To incorporate the possibility that a cell may be in the process of transitioning toward a given phenotype, we categorized cells by their previously identified Monocle state (progenitor, effector, or exhausted). We then plotted the quantitative affinity of each clone against the percent of cells with an exhausted Monocle state in the clone (Fig. S4 B). Interestingly, there was no linear correlation between these variables ($P = 0.83$), suggesting TCR affinity may not directly impact cellular differentiation in chronic infection. However, our scRNA-seq data provided deeper insight into this relationship, or lack thereof. We noticed that exhausted cells displayed higher expression of TCR constant chain genes compared to other clusters (Fig. 6 B) and also expressed higher levels of most CD3 genes (Fig. S4 C). Taken together, these trends in gene expression led us to speculate that exhausted cells may have higher numbers of TCRs on their cell surfaces and thus have higher binding avidities, rather than binding affinities, compared to effector cells.

By taking a product of quantitative affinity and TCR constant chain gene expression, we calculated a metric we termed quantitative avidity (see Materials and methods). We then plotted clonal quantitative avidity against the percent of exhausted cells per clone, which revealed a significant positive linear correlation ($P = 0.032$, $R = 0.22$; Fig. 7 C). Plotting clonal quantitative avidity against the percentage of effector cells per clone also showed a significant correlation, but one that was negative rather than positive ($P = 0.0009$, $R = -0.36$; Fig. 7 D). Conversely, and consistent with our analysis of quantitative affinity in relation to an exhausted cell fate, examining quantitative affinity of clones in relation to percent effector Monocle state per clone also showed no correlation ($P = 0.69$; Fig. S4 D). We confirmed that these trends in avidity among the different phenotypes were consistent on a per cell basis in addition to a per clone basis. Doing so provided an ordering of Monocle states by quantitative avidity, with exhausted cells having significantly

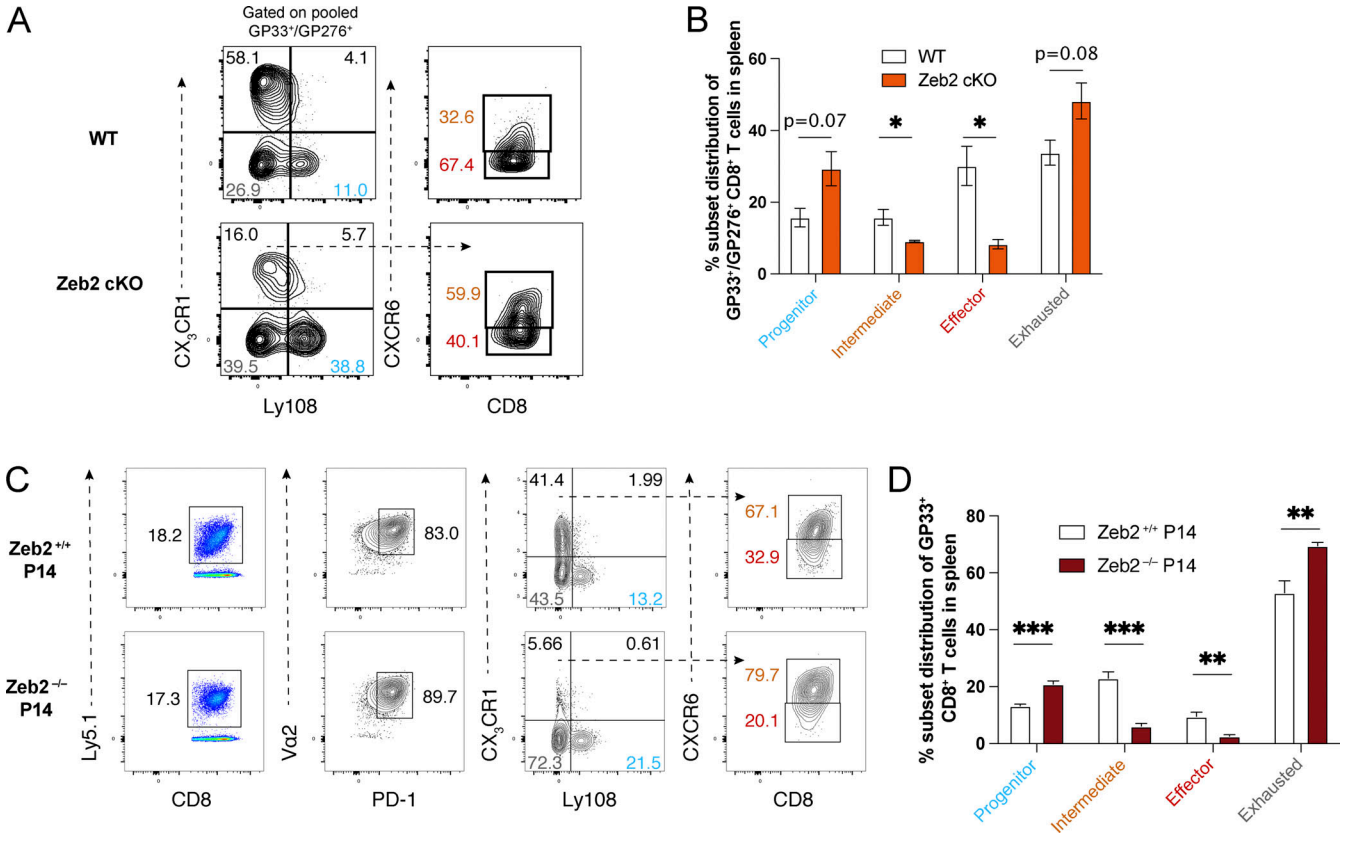

Figure 6. **The TF Zeb2 is intrinsically required for differentiation of effector CD8⁺ T cells. (A and B)** Representative flow plots (A) and summary data(B) showing the frequencies of GP33/GP276 antigen-specific CD8⁺ T cell subsets collected from spleens of WT ($Zeb2^{flox/flox}$ GzB-Cre^{-}) or Zeb2 cKO ($Zeb2^{flox/flox}$ GzB-Cre^{+}) mice on day 30 p.i. with LCMV Clone 13. **(C and D)** Representative flow plots (C) and summary data (D) showing the proportion of $Zeb2^{+/+}$ and $Zeb2^{-/-}$ P14 CD8⁺ T cells with a progenitor, intermediate, effector, or exhausted phenotype. P14 cells were adoptively transferred 1 d before LCMV Clone 13 infection and analyzed 18 d p.i. Data (mean ± SEM) in B are from three mice per group and are representative of two independent experiments. Data (mean ± SEM) in D are from five mice per group and are representative of two independent experiments. * $P < 0.05$, ** $P < 0.01$, *** $P < 0.001$.

higher quantitative avidity than effector cells ($P = 5 \times 10^{-19}$; Fig. S4 E). As binding avidity is known to correlate with increased signaling through multiple pathways downstream of the TCR (Conley et al., 2016), we calculated module scores of TCR signaling genes within our Seurat clusters using the "T cell receptor signaling pathway" gene set from GSEA (Kyoto Encyclopedia of Genes and Genomes [KEGG] hsa04660). We found that TCR signaling module scores were significantly higher in exhausted cells and significantly lower in effector cells compared to all other clusters (Fig. 7 E), further validating our quantitative avidity model.

As tetramer binding has been shown to positively correlate with TCR avidity (Yee et al., 1999), we recapitulated our in silico findings ex vivo by running flow cytometry on LCMV GP33-specific murine splenic CD8⁺ T cells harvested 30 d p.i. with LCMV Clone 13 (Fig. 7 F). High-avidity ($GP33^{hi}$) CD8⁺ T cells had a significantly higher proportion of exhausted cells ($P < 0.05$) and a significantly lower proportion of effector cells ($P < 0.05$) compared to low-avidity ($GP33^{lo}$) CD8⁺ T cells (Fig. 7 G). Interestingly, progenitor cells were also enriched in high-avidity versus low-avidity CD8⁺ T cells, but there was no significant difference in the proportions of intermediate cells. Within the entire GP33⁺ CD8⁺ T cell population, the MFI of GP33 tetramer was also significantly higher in exhausted cells compared to both intermediate cells ($P < 0.05$) and effector cells ($P < 0.05$; Fig. 7 H). Together, our computational models, scRNA-seq TCR signaling metrics, and tetramer binding measurements from flow cytometry collectively suggest that variations in TCR avidity and downstream signal strength correlate with CD8⁺ T cell differentiation states in the setting of chronic viral infection.

SHP-1 intrinsically maintains progenitor CD8⁺ T cell quiescence and limits effector cell differentiation

Our results demonstrate a robust positive association between CD8⁺ T cell binding avidity, TCR signaling, and an exhausted differentiation state. These findings also suggest that CD8⁺ T cells with lower avidity, and consequently lower TCR signaling, may be shielded from an exhausted T cell fate. Intriguingly, and in line with this idea, our scRNA-seq analyses further identified that *Ptpn6* (encodes SHP-1), a phosphatase known to antagonize TCR signaling (Pani et al., 1996), was the only gene from the TCR signaling gene set (KEGG hsa04660) significantly upregulated in both progenitor and effector cells but downregulated in exhausted cells (Fig. S5 A). Previous findings indicate that SHP-1 activity is increased upon weak ligand binding,

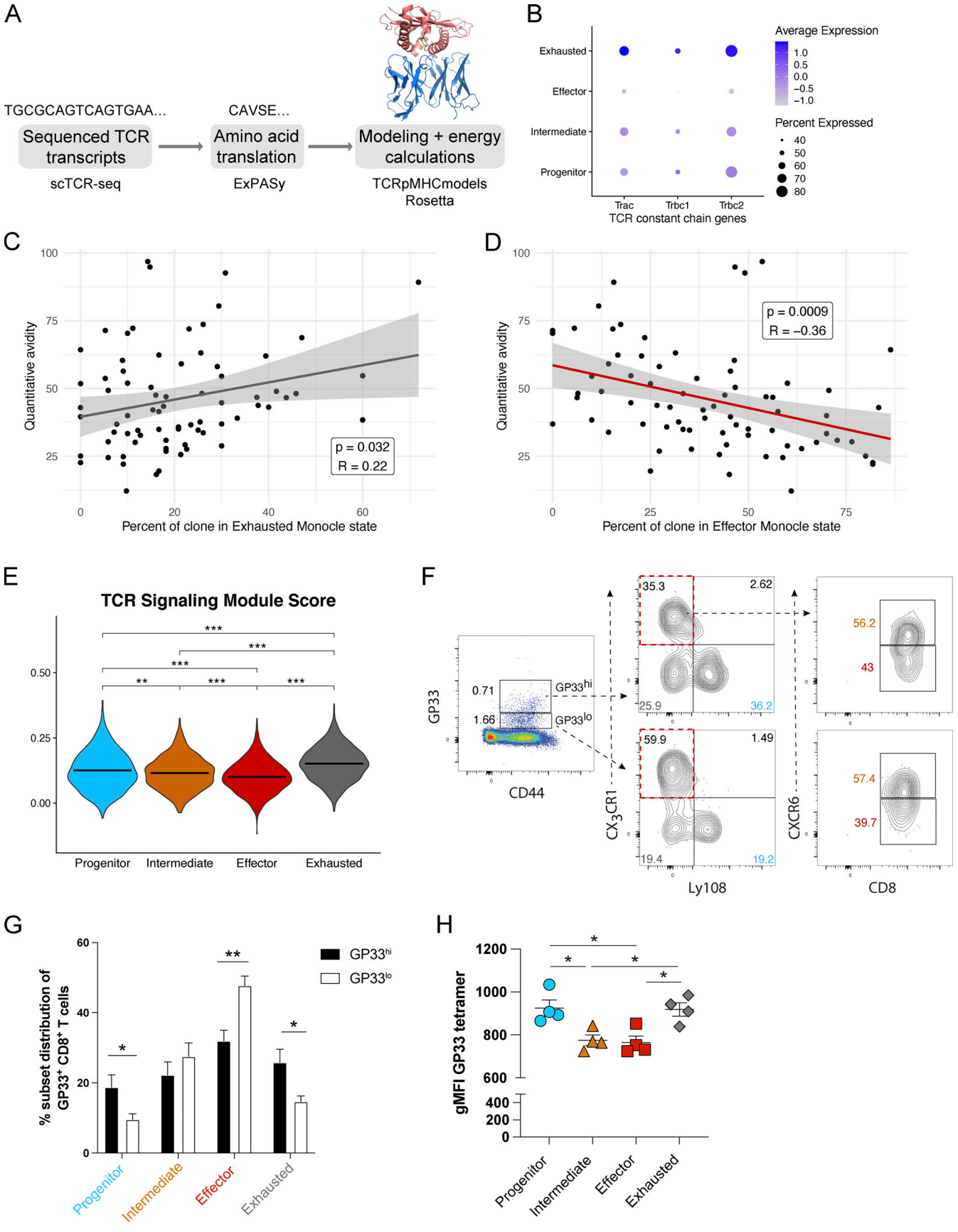

Figure 7. **TCR:pMHC quantitative avidity correlates with phenotypic skewing of CD8⁺ T cell clones. (A)** Diagram of TCR modeling workflow. **(B)** Dot plot showing TCR constant chain gene expression per cluster. Dot size, percent of cells expressing each gene; color, scaled expression. **(C)** Linear regression

between quantitative avidity and percent of cells per clone in the exhausted Monocle state. Each point represents one clone. Gray shaded region, 95% confidence interval. **(D)** As in C but with the percent of cells per clone in the effector Monocle state. **(E)** Violin plot of TCR signaling module scores calculated using a published gene set (KEGG hsa04660). Horizontal black lines denote mean values. **(F and G)** Representative flow plots (F) and summary data (G) showing subset distributions of GP33^{hi} (high avidity) and GP33^{lo} (low avidity) splenic CD8$^+$ T cells harvested 30 d p.i. with LCMV Clone 13. **(H)** Quantification of GP33 MFI in subsets from F. Data (mean ± SEM) in G and H are from four mice and are representative of at least four independent experiments. * P < 0.05, ** P < 0.01, *** P < 0.001. gMFI, geometric MFI. See also Fig. S4.

whereas strong TCR agonists prevent SHP-1 recruitment to the TCR complex, thereby allowing downstream signaling to continue (Štefanová et al., 2003). Moreover, it has further been suggested that TCR signaling cascades will continue unimpeded until SHP-1 expression levels reach a critical threshold (Feinerman et al., 2008). As exhausted CD8$^+$ T cells exhibit higher avidity and greater TCR signal strength while effector CD8$^+$ T cells have lower avidity and TCR signal strength (Fig. 7, C–E), we hypothesized that an inverse correlation existed between TCR avidity and SHP-1 activity. Consistent with previous findings and our hypothesis, our data demonstrated that *Ptpn6* expression levels are inversely correlated with CD8$^+$ T cell quantitative binding avidity (Fig. 8 A). Furthermore, Monocle trajectory analysis showed that although *Ptpn6* expression is highest among progenitor cells, it is also stably maintained in the effector subset, whereas exhausted cells display rapid loss of *Ptpn6* expression in pseudotime (Fig. S5 B). Taken together, these findings led us to hypothesize that SHP-1 expression is required to maintain the progenitor CD8$^+$ T cell subset in a quiescent-like state, while also serving to limit the accumulation of lower-avidity effector cells.

To test this, we infected groups of *Ptpn6*$^{flox/flox}$ dLck-Cre$^-$ and *Ptpn6*$^{flox/flox}$ dLck-Cre$^+$ mice with LCMV Cl13 and assessed virus-specific CD8$^+$ T cell responses on day 28 p.i. by flow cytometry (Fig. S5 C). Notably, abrogation of SHP-1 resulted in approximately a 50% increase in the accumulation of GP33-specific CD8$^+$ T cells in the spleen (Fig. S5, C and D). Importantly, this increase was largely attributable to selective outgrowths of cells, as evidenced by ∼40–50% increases in the proportions of effector and intermediate virus-specific CD8$^+$ T cells (Fig. S5 E), as well as a significant increase in the proportion of low-avidity GP33^{lo} tetramer-binding CD8$^+$ T cells (Fig. S5, F and G). As expected, these observed increases in effector cell responses were further accompanied with concomitant decreases in the proportion of progenitor CD8$^+$ T cells in *Ptpn6*$^{flox/flox}$ dLck-Cre$^+$ mice (Fig. S5 E), indicating that SHP-1 may help insulate progenitor CD8$^+$ T cells from acquiring a more terminal differentiation state. In accordance with these observations, virus-specific CD8$^+$ T cells from *Ptpn6*$^{flox/flox}$ dLck-Cre$^+$ mice displayed an augmented capacity to degranulate and produce IFN-γ in response to ex vivo GP33 peptide stimulation (Fig. S5 H). Of note, no consistent differences in the proportion of exhausted CD8$^+$ T cells (Fig. S5 E) or expression of co-inhibitory receptors PD-1, Tim3, 2B4, and Lag3 on GP33-specific CD8$^+$ T cells (Fig. S5 I) were observed between experimental groups.

One limitation of these experiments was that SHP-1 was ablated in both CD4$^+$ and CD8$^+$ T cells. To strengthen these findings, we examined the CD8$^+$ T cell–intrinsic role of SHP-1 by generating MBM chimera mice in which lethally irradiated WT Ly5.1 mice were reconstituted with bone marrow from CD8$^{-/-}$ mice (70%) and either *Ptpn6*$^{f/f}$ dLck-Cre$^+$ (cKO) or *Ptpn6*$^{f/f}$ dLck-Cre$^-$ (WT) mice (30%; Fig. 8 B). Following reconstitution, the mice were infected with LCMV Clone 13 and spleens were harvested 21 d p.i. (Fig. 8 C). Although we did not observe any significant changes in the frequency of total GP33$^+$ CD8$^+$ T cells (Fig. 8 D), we did once again notice a selective and statistically significant increase in the frequency of low-avidity GP33^{lo} cells (Fig. 8 E). Furthermore, although we did not observe a significant increase in the proportion of intermediate cells, there was still a significant reduction (∼50%) in the frequency of progenitor cells and an almost twofold increase in the frequency of effector cells (Fig. 8 F). The frequency of exhausted cells was also once again unchanged. When examining absolute cell numbers, we found a significant increase only in the number of effector cells while the other subsets were unchanged (Fig. S5 J), further supporting our hypothesis that SHP-1 ablation selectively enables the outgrowth of effector cells. In line with this, we found that CD8$^+$ T cells from mice reconstituted with SHP-1 cKO bone marrow had a significantly increased capacity to produce TNFα and IFN-γ following ex vivo GP33 peptide stimulation (Fig. 8 G). To generalize our findings, we also examined CD8$^+$ T cells specific for the LCMV epitopes GP276 and NP396. We found no differences in the frequency of NP396$^+$ cells between SHP-1 cKO and SHP-1 WT CD8$^+$ T cells, although the frequency of GP276$^+$ cells was reduced among SHP-1 cKO CD8$^+$ cells compared to WT (Fig. S5 K). Frequencies of individual subsets, however, followed similar trends regardless of antigen specificity. GP276-specific SHP-1 cKO CD8$^+$ T cells exhibited a significantly reduced proportion of progenitor cells and a ∼30% reduction in the frequency of exhausted cells that approached significance, while effector cell frequency was significantly increased nearly twofold (Fig. S5 L). NP396-specific SHP-1 cKO CD8$^+$ T cells had significantly reduced frequencies of exhausted cells and intermediate cells, as well as a significant threefold increase in the frequency of effector cells (Fig. S5 M). Minor differences in subset or antigen-specific CD8$^+$ T cell frequencies in various antigen-specific CD8$^+$ T cells following SHP-1 deletion may be the result of a variety of confounding factors, including variations in immunodominance against the three major LCMV epitopes as well as different affinities and avidities of these epitopes for TCRs. Taken together, our data indicate that SHP-1 expression is more abundant in lower avidity T cells and that CD8$^+$ T cell-intrinsic SHP-1 activity may function to help preserve the progenitor CD8$^+$ T cell subset while it simultaneously selectively restricts the accumulation of effector CD8$^+$ T cells. Thus, inhibition of SHP-1, as well as manipulation of other signaling pathways identified in this study, may serve as a useful

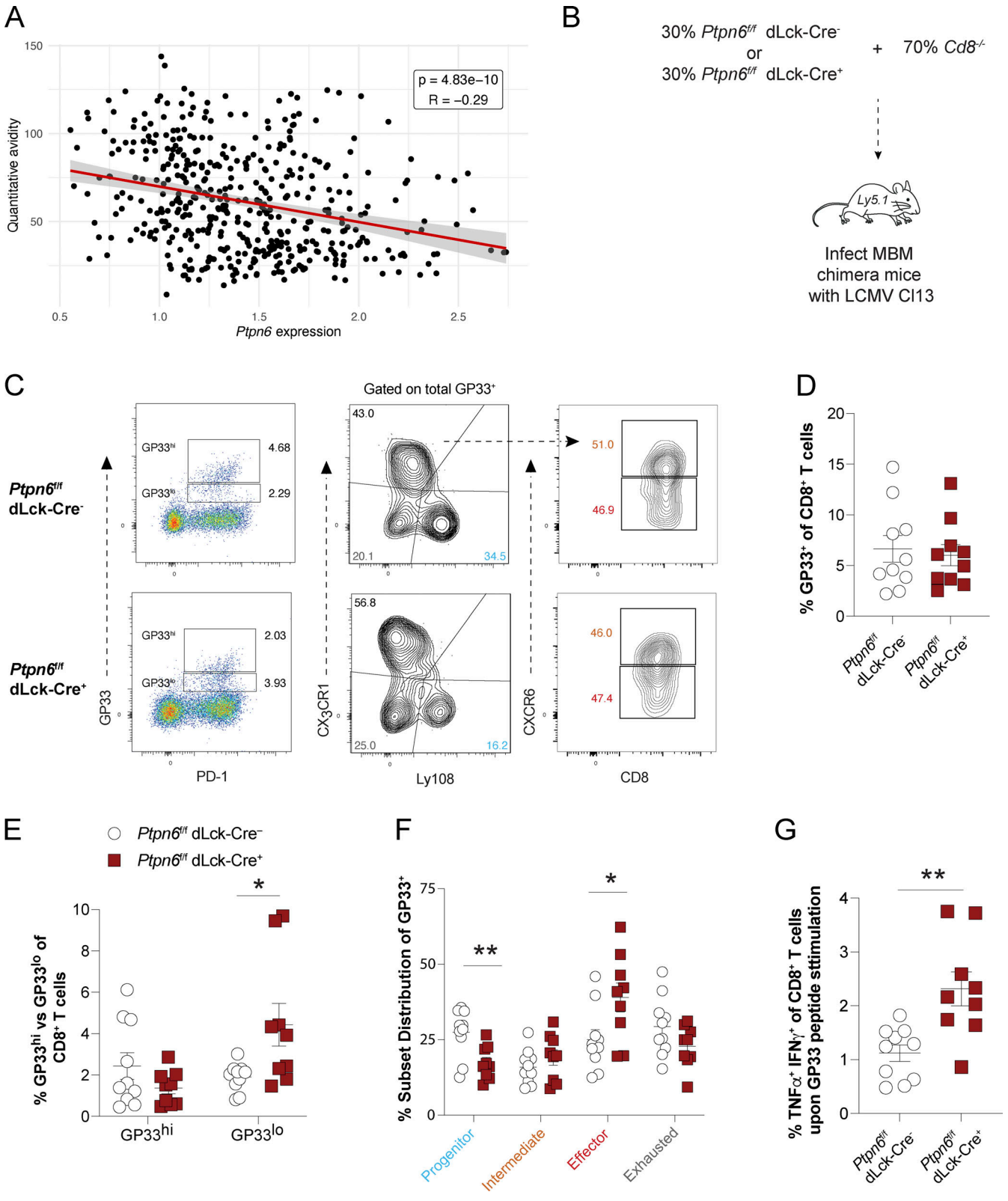

Figure 8. **SHP-1 intrinsically maintains progenitor CD8⁺ T cell quiescence and limits effector cell differentiation. (A)** Linear regression between quantitative avidity and expression of *Ptpn6* (encodes SHP-1). Gray shaded region, 95% confidence interval. Each point denotes one cell. Cells with 0 reads of *Trac*, *Trbc1*, *Trbc2*, or *Ptpn6* were excluded. **(B)** Experimental design for SHP-1 MBM chimera studies. **(C)** Representative flow plots of splenic CD8⁺ T cells harvested from *Ptpn6*$^{flox/flox}$ dLck-Cre⁻ or *Ptpn6*$^{flox/flox}$ dLck-Cre⁺ MBM chimera mice. **(D)** Summary of frequency of GP33⁺ splenic CD8⁺ T cells in C. **(E)** Summary of frequency of GP33^{hi} and GP33^{lo} CD8⁺ T cells in C. **(F)** Quantification of subset proportions from C. **(G)** Frequency of TNFα⁺ IFNγ⁺ CD8⁺ T cells upon ex vivo stimulation with GP33 peptide. Data (mean ± SEM) in D–G are from five mice per group and are pooled from two independent experiments. * P < 0.05, ** P < 0.01. See also Fig. S5.

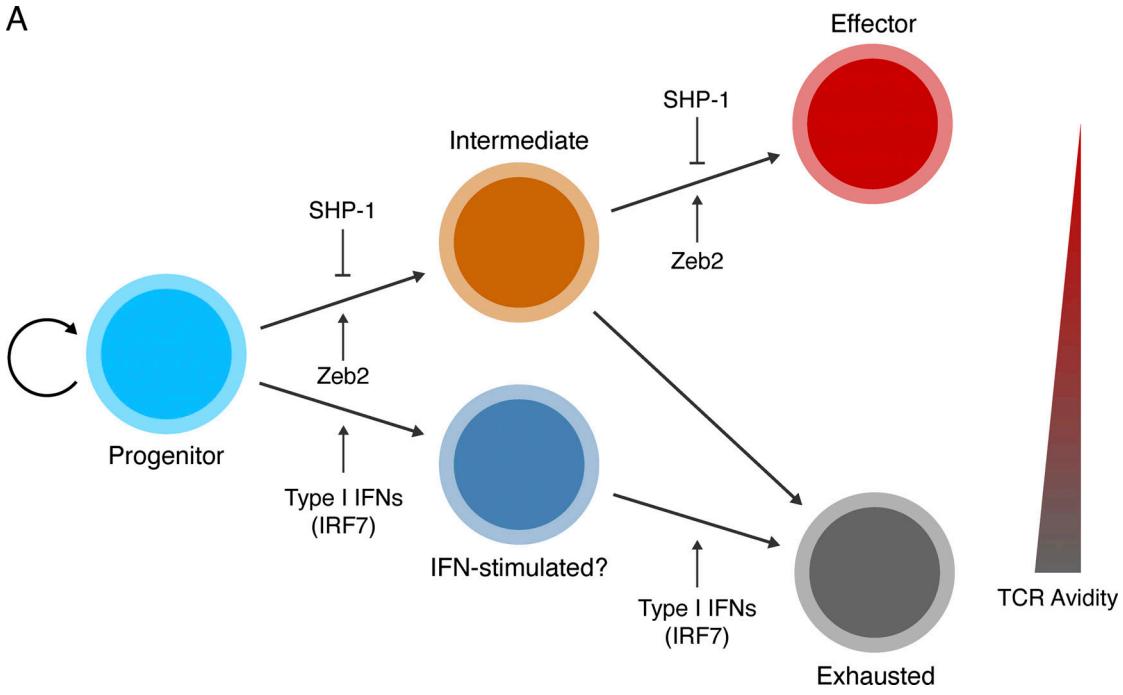

Figure 9. **Model of CD8⁺ T cell differentiation during chronic viral infection. (A)** Five subset bifurcative model of CD8⁺ T cell differentiation during chronic viral infection. Various signaling pathways and transcription factors affect CD8⁺ T cell quiescence, differentiation, and fate decisions. Some data indicate the existence of an IFN-stimulated subset that acts as a direct transition state between progenitor and exhausted cells.

strategy to generate more cytolytic effector CD8⁺ T cells to improve control over chronic viral infection or cancer (Fig. 9 A).

Discussion

In this study, using scRNA-seq and scTCR-seq analyses to identify CD8⁺ T cell clones by their unique paired TCR α and β chain sequences, we demonstrate that CD8⁺ T cells responding to chronic viral infection display clonotypic and transcriptional heterogeneity. Merging single-cell clonotypic and transcriptomic data sets together empowered us to track the lineage commitment and differentiation trajectory of each clone from multiple endogenous GP33-specific CD8⁺ T cell repertoires. Notably, our data show that the TCRs that define individual T cell clones are incredibly diverse, as there was no clonal overlap between multiple genetically identical organisms when defining clones by paired TCR α and β chain sequences. In addition, our study indicates that most CD8⁺ T cell clones appear multi-fated, thus answering a long-standing question about clonal fate from an endogenous non-transgenic CD8⁺ T cell repertoire. However, we also found that the probability of assuming a particular terminal fate can be influenced by various factors, as some clones appear to exhibit preferential skewing toward a particular lineage. Our data suggest that this fate decision may in part be influenced by environmental and inflammatory cues propagated during persistent infection, TCR avidity, and signaling cascades downstream of the TCR. These data imply that the use of LCMV-specific TCR transgenic P14 CD8⁺ T cells may therefore alter or negate the impact of TCR structural heterogeneity, avidity, and signaling on CD8⁺ T cell differentiation, although further work will be required to investigate this mechanistically. Collectively, our data from single-cell sequencing analyses and in vivo experiments are supportive of a bifurcation model of CD8⁺ T cell differentiation during chronic viral infection, with TCF-1⁺ progenitor cells transitioning through the CX_3CR1^+ CXCR6⁺ intermediate population to become either terminally differentiated CX_3CR1^+ $CXCR6^-$ effector or PD-1^{hi} exhausted cells. Our data also reveal a small IFN-stimulated population which may act as a direct transition state between progenitor and exhausted cells, thus suggesting that there may be multiple distinct differentiation pathways to exhaustion. Our study sheds further light on these distinct developmental pathways using multiple computational tools and subsequent in vivo validation experiments to closely examine the progenitor and intermediate CD8⁺ T cell populations and the signaling pathways that impact their propensity to generate either effector or exhausted cells.

Intermediate cells arise from progenitor cells and seem to be capable of giving rise to either effector or exhausted cells, as suggested by fate tracing analyses and validated by adoptive transfer experiments. These cells were predicted to be less quiescent than progenitor cells, having greater spread across pseudotime in trajectory analysis and increased metrics of clonal expansion and inter-cluster transition. Accordingly, in the time frame examined, they were more capable than progenitor cells of developing a terminally differentiated effector or exhausted phenotype upon adoptive transfer to infection-matched mice. However, the adoptive transfer experiments we performed have their limitations. Recent work has shown that the differentiation of progenitor CD8⁺ T cells may be suppressed by

type 1 conventional dendritic cells (cDC1s) in secondary lymphoid tissue (Dähling et al., 2022). Removing progenitor cells from this structured immunoregulatory niche and placing them in the blood through intravenous transfer may therefore expose them to TCR and cytokine signaling and impact their differentiation. Previous work has lineage traced effector-like CD8⁺ T cells in chronic infection using the marker CX_3CR1 (Raju et al., 2021). However, further work will be needed to fully understand the differentiation of CD8⁺ T cells, particularly effector-like cells, in the early timepoint of chronic infection and how effectively these cells can persist during the late stage of infection. In addition, fate mapping with both CX_3CR1 and CXCR6 may further clarify how progenitor cells ultimately differentiate toward either an effector or exhausted cell fate. However, given the intermediate cluster's large size (28.2% of total cells), its high level of clonal overlap with both effector and exhausted cells, its high degree of predicted transition potential with both terminally differentiated clusters, and the capacity of these cells to generate both terminally differentiated effector and exhausted cells in vivo, it seems likely that intermediate cells represent a bifurcation of CD8⁺ T cell differentiation during chronic viral infection, although this may not be the only branch point on the road to exhaustion.

Previously published findings indicate that CD8⁺ T cell–intrinsic type I IFN signaling at least in part contributes to decreased progenitor CD8⁺ T cell formation (Wu et al., 2016) and that blockade of type I IFN signaling restores secondary lymphoid architecture, augments TCF-1^{hi} progenitor CD8⁺ T cell formation (Huang et al., 2019), enhances CD8⁺ T cell effector function, and improves viral control during chronic viral infection (Wilson et al., 2013; Teijaro et al., 2013). However, our data build upon these concepts by specifically elucidating that induction of prolonged type I IFN signaling, such as through Poly (I:C) administration, forces progenitor cells to selectively develop into exhausted cells and that this differentiation may occur through the IFN-stimulated population. Additionally, we show that genetic ablation of the TF IRF7 maintains higher levels of progenitor cells and decreases exhausted cell formation. Taken together, these data indicate that prolonged exposure to type I IFN signaling, a cardinal feature of chronic viral infection (Snell et al., 2017), drives progenitor CD8⁺ T cell differentiation directly toward exhaustion through an IRF7-dependent mechanism, potentially bypassing intermediate cells and the possibility of generating effector cells altogether. Conversely, we found that the TF Zeb2, which has previously been shown to be important for the terminal differentiation of CD8⁺ T cells in acute viral infection (Omilusik et al., 2015), is also critical for the terminal differentiation of effector cells during chronic viral infection. Our recent work has also shown that the TFs BATF and T-bet are critical for effector cell generation during chronic viral infection, potentially by regulating Zeb2 (Chen et al., 2021). However, we have also previously been shown that Zeb2 has functions independent of T-bet in acute viral infection (Dominguez et al., 2015). Therefore, further study of the functions of Zeb2 is warranted to better understand effector cell differentiation during chronic viral infection. Our data therefore add to previous observations by ourselves and others identifying and characterizing terminally differentiated effector cells that comprise a large proportion of the CD8⁺ T cell pool during the late stage of chronic infection (Zander et al., 2019; Raju et al., 2021; Sandu et al., 2020). More broadly, identifying regulators of effector and exhausted cell fates may have important implications for strategies aimed at bolstering CD8⁺ T cell responses during chronic infection and cancer, as attempts to limit exhaustion and bolster antiviral or antitumor CD8⁺ T cell activity may benefit from targeting multiple independent pathways rather than only one.

Our data indicate that the differentiation trajectory of progenitor CD8⁺ T cells in chronic infection may be influenced by various factors. We have previously demonstrated that CD4⁺ T cell help through IL-21 production is necessary for effector CD8⁺ T cell differentiation (Zander et al., 2019), and we have discussed above that increased type I IFN signaling selectively promotes the development of an exhausted phenotype through the induction and activity of IRF7, potentially through the IFN-stimulated subset. In addition, here we have investigated the roles of TCR avidity and signal strength as well as SHP-1 phosphatase activity. Intriguingly, our data suggest that TCR:pMHC binding avidity plays a more dominant role than TCR:pMHC binding affinity in shaping the phenotypic skewing of CD8⁺ T cell clones. Moreover, two recent studies have used bulk TCR-seq to demonstrate that TCF-1⁻ cells (non-progenitors) and TCF-1⁺ cells (progenitors) have major TCR clonal overlap (Yermanos et al., 2020) and that the TCR repertoire shrinks over the course of chronic LCMV infection (Chang et al., 2020). The former observation supports our scTCR-seq analysis suggesting that progenitor cells seed the CD8⁺ T cell pool during the late stage of chronic LCMV infection. The latter observation, in combination with our observation of a lack of correlation between affinity and CD8⁺ T cell fate in the chronic stage of LCMV Clone 13 infection, suggests there may be a temporal TCR affinity-based clonal selection pressure during the early stages of chronic infection. These findings are consistent with a previous report demonstrating that antigen amount was a key determinant of T cell dysfunction whereas TCR affinity played a negligible role, as even persistent low-affinity TCR stimulation was sufficient to induce an exhausted phenotype (Utzschneider et al., 2016a). On the other hand, increased avidity allows for larger numbers of durable TCR:pMHC interactions and leads to increased levels of TCR signaling downstream of ligand binding (Allard et al., 2017). In line with this, our data suggest that clones with higher binding avidities have a greater propensity for generating exhausted cells, whereas those with lower binding avidities are skewed toward developing into effector cells. These observations parallel a recent study demonstrating that high-affinity CD8⁺ T cell clones responding to persistent human CMV infection contract to a greater extent relative to the overall population due to their development of a senescent phenotype (Schober et al., 2020). It is important to note that the impact of binding avidity on cell fate in our data was graded rather than binary, with most CD8⁺ T cell clones appearing to be multi-fated and capable of developing both effector and exhausted cells after transitioning through the intermediate phenotype. Thus, these data favor a "one (progenitor) cell, multiple fate" model similar

to what has been demonstrated for CD8⁺ T cells (Gerlach et al., 2010) and CD4⁺ T cells (Khatun et al., 2021) in acute viral infection; however, our model also acknowledges the impact of phenotypic skewing on individual clones by factors such as TCR avidity and signal strength as well as signals received through the cytokine milieu present in chronic infection.

The impact of TCR avidity on CD8⁺ T cell phenotype may extend beyond chronic viral infection. It has been shown that vaccination with tumor peptides modified to have higher TCR affinity leads to increased TCR:pMHC dwell time, persistent increased PD-1 protein expression, and ultimately decreased antitumor efficacy of CD8⁺ T cells (Zahm et al., 2017). Conversely, CD8⁺ T cells primed with low-affinity antigen are known to acquire cytotoxic function earlier than those primed with high-affinity antigen (Ozga et al., 2016). These data are in agreement with our findings, which show that exhausted CD8⁺ T cells exhibit increased TCR avidity for pMHC and have increased expression of TCR signaling genes, whereas effector cells exhibit lower TCR avidity and decreased TCR signaling. Multiple TFs known to be associated with the development of an exhausted phenotype, such as Tox (Khan et al., 2019), Nur77 (Liu et al., 2019), IRF4 (Man et al., 2017), and NFAT (Martinez et al., 2015), are also activated downstream of TCR signaling. Increased avidity may allow for increased TCR signaling and thus an increase in exhaustion-inducing TF activity, though further work will be required to elucidate the precise mechanisms and kinetic nuances of these pathways.

Intriguingly, our data also show that expression levels of *Ptpn6*, which encodes the phosphatase SHP-1, are inversely associated with CD8⁺ T cell quantitative TCR avidity. Previous research indicates that SHP-1 may negatively regulate TCR signaling, with SLP-76, Zap70, and Lck all being potential substrates. Notably, several studies have suggested a role for SHP-1 in discriminating between agonistic and antagonistic TCR signaling (Hebeisen et al., 2013; Lorenz, 2009; Štefanová et al., 2003; Feinerman et al., 2008). Under conditions of weak ligand binding, it has been proposed that Lck phosphorylates SHP-1 on Y564, thereby resulting in the rapid recruitment of SHP-1 to the TCR complex through binding of the Lck SH2 domain to phosphorylated SHP-1 (Štefanová et al., 2003). Subsequently, SHP-1 can then dephosphorylate and inactivate Lck kinase, resulting in receptor desensitization. Conversely, with strong TCR agonists, activated ERK kinase phosphorylates Lck at Serine 59, which inactivates the SH2 domain and prevents recruitment of SHP-1 to the TCR complex, thereby allowing downstream signaling to continue. Moreover, it has further been suggested that TCR signaling cascades will continue unimpeded until SHP-1 expression levels reach a critical threshold (Feinerman et al., 2008). Taken together, these observations led us to speculate that exhausted CD8⁺ T cells, which exhibit higher avidity, increased ligand binding, and greater TCR signal strength, will experience reduced recruitment of SHP-1 to the TCR complex, and as such may be less susceptible to SHP-1 mediated inhibition. By contrast, as *Ptpn6* expression was largely only detected in the progenitor and effector CD8⁺ T cell subsets, we speculated that abrogation of SHP-1 activity would selectively uncouple the inhibition of these two respective subsets, thereby enabling the selective outgrowth of effector cells while having only a minor impact on higher-avidity exhausted cells. Indeed, we demonstrate here that CD8⁺ T cell–intrinsic loss of SHP-1 augments effector CD8⁺ T cell differentiation at the expense of maintaining the progenitor pool of CD8⁺ T cells, while further leaving the exhausted pool largely unchanged during chronic viral infection. As SHP-1 has also previously been identified to limit effector cell accumulation during acute viral infection and cancer (Fowler et al., 2010; Stromnes et al., 2012), we propose that SHP-1 activity may be a conserved regulatory mechanism that constrains effector CD8⁺ T cell development and function. As such, therapeutically targeting SHP-1 may allow for a tailored approach to augment effector CD8⁺ T cell differentiation and enhance viral or tumor control (Snook et al., 2020). Another recent study has shown that the protein Trib1, which negatively regulates TCR signaling, also inhibits the generation of KLRG1⁺ effector-like cells during chronic LCMV infection (Rome et al., 2020). Although this study did not test whether Trib1 selectively acts on low-avidity progenitor cells, the parallels between SHP-1 and Trib1 suggest that inhibiting TCR signaling in CD8⁺ T cells may be beneficial for viral control during chronic infections.

Our SHP-1 experiments also suggest that certain subsets of progenitor cells may normally be more quiescent than others, as ablation of SHP-1 mobilizes certain progenitor cells selectively toward an effector fate. This is in agreement with both our scTCR-seq data, which show an increased level of clonal diversity in progenitor cells compared to all other subsets, as well as another recently proposed model of CD8⁺ T cell differentiation in chronic infection (Beltra et al., 2020). This finding also agrees with recent bulk TCR-seq experiments showing that the CD8⁺ T cell clonal repertoire narrows over the course of chronic LCMV infection and is broader in TCF-1^{hi} progenitor cells than PD-1^{hi} exhausted cells (Chang et al., 2020). Taken together, these observations suggest a link between TCR avidity, TCR signaling, and CD8⁺ T cell lineage commitment during chronic viral infection. Nevertheless, the underlying mechanisms by which TCR avidity and downstream TCR signaling pathways, including SHP-1 phosphatase activity, impact cell fate decisions warrant further study, as these have implications for topics ranging from control of chronic viral infection to optimal design of chimeric antigen receptor T cells for cancer immunotherapy.

Collectively, this multifaceted process of CD8⁺ T cell differentiation, wherein progenitor CD8⁺ T cells sustain the pool of both terminal effector and exhausted CD8⁺ T cell subsets by progressing through the bifurcating intermediate phenotype, likely exemplifies a functional adaptation process that occurs when antigen presentation and inflammatory signals are persistent, such as during chronic infection and cancer. Moreover, we speculate that this division of labor is likely essential to maintain viral or tumor control, while simultaneously limiting excessive immunopathology. Work in mice has shown that the development of exhausted cells is vital to protect the host against immunopathology during chronic viral infection (Cornberg et al., 2013). Conversely, the administration of immune checkpoint blockade therapy such as anti–PD-1 to human patients, which aims to skew the T cell pool toward an effector-like phenotype for tumor lysis, is known to cause autoimmune

adverse effects (Michot et al., 2016). The delicate balance between effector and exhausted CD8⁺ T cell development and function is also illustrated well by cancer immunotherapy, as multiple clinical trials have demonstrated that the development of autoimmune reactions following anti–PD-1 therapy actually correlates with improved response rates and progression-free survival in several different tumor types (Sato et al., 2018; Okada et al., 2019; Elias et al., 2019). In addition, a recent study has shown that CD3ε limits cytokine storm by reducing TCR signaling when added to chimeric antigen receptor T cell constructs (Wu et al., 2020). This finding further links TCR signal strength to functional differences in CD8⁺ T cells, similar to our data showing that SHP-1 selectively restricts the formation of low-avidity effector cells from progenitor cells, potentially to protect against immunopathology. Therefore, a further understanding of the precise mechanisms underlying the differentiation of the effector and exhausted CD8⁺ T cell subsets, including factors such as type I IFN signaling, TF function, SHP-1 activity, and TCR signaling that selectively favor progenitor cell bifurcation toward one or the other through the intermediate population, and possibly also the IFN-stimulated CD8⁺ T cell population, will be crucial in order to develop more nuanced therapeutics for cancer and chronic viral infection with fewer immunopathologic adverse effects.

Materials and methods

Mice and LCMV infection

6–8-wk-old male and female C57Bl/6 mice were used for all experiments, unless otherwise indicated. *Ptpn6*$^{fl/fl}$ dLck-Cre^{-} and *Ptpn6*$^{fl/fl}$ dLck-Cre^{+} mice were kindly provided by Dr. Vera Tarakanova (Medical College of Wisconsin [MCW], Milwaukee, WI) and Dr. Ulrike Lorenz (University of Virginia, Charlottesville, VA). All mice were bred and maintained under the guidelines of the Institutional Animal Care and Use Committees of the MCW, Yale University (animal protocol number 20112), the Salk Institute, and the University of Virginia. Mice were infected with 2 × 10^{6} PFU of LCMV strain Clone 13 (Cl13) through retroorbital injection to establish chronic viral infection.

Granzyme B-Cre (GzB-Cre^{+}) mice were provided by J. Jacobs (Emory University, Atlanta, GA) through R. Flavell's laboratory (Yale University School of Medicine, New Haven, CT) and were crossed to Zeb2$^{flox/flox}$ mice for generation of GzB-Cre^{+}Zeb2$^{flox/flox}$ (Zeb2$^{-/-}$) mice and GzB-Cre^{-}Zeb2$^{flox/flox}$ (Zeb2$^{+/+}$) mice. Zeb2$^{-/-}$ and Zeb2$^{+/+}$ mice were further crossed to P14 (Ly5.1/5.1) TCR transgenic mice so that P14 Zeb2$^{-/-}$ and P14 Zeb2$^{+/+}$ mice could be obtained.

SHP-1$^{flox/flox}$ (*Ptpn6*$^{f/f}$) mice (Pao et al., 2007) were crossed to distal Lck-Cre (dLck-Cre) mice (Zhang et al., 2005). Genotyping of all mice was done by PCR as described previously for the *Ptpn6*$^{f/f}$ allele and dLck-Cre allele.

Administration of biologics

In some experiments, LCMV Cl13-infected WT mice were administered 200 µg of Poly (I:C) (Sigma-Aldrich) on days 14, 16, 18, and 23 p.i. In other sets of experiments, mice were administered 100 µg of Poly (I:C), with similar results being observed.

Flow cytometry

Single-cell suspensions were incubated with antibodies against surface markers for 30 min at 4 degrees, followed by 3× washing in FACS buffer. These samples were then run on an LSR II Green flow cytometer (BD Biosciences) and analyzed by FlowJo software (BD Biosciences).

Intracellular TF staining: After surface staining, cells were fixed with buffer from the True-Nuclear Transcription Factor Buffer Set (BioLegend) for 1 h. Then cells were then washed with permeabilization buffer and stained with antibodies against transcription factors in permeabilization buffer.

Intracellular cytokine staining: Single-cell suspensions were stimulated with GP33 peptide in the presence of brefeldin A (BioLegend). Subsequently, cells were collected to stain for surface markers and fixed by fixation buffer (BioLegend). Cells were then washed with permeabilization buffer (BioLegend) and stained for cytokine-specific antibodies in permeabilization buffer.

Cell transfer experiments

Ly108^{+}CX$_3$CR1^{-} (progenitor), CX$_3$CR1^{+}CXCR6^{+} (intermediate), CX$_3$CR1^{+}CXCR6^{-} (effector), and CX$_3$CR1^{-}Ly108^{-}PD-1^{hi} (exhausted) CD8⁺ T cell subsets were sorted from LCMV Cl13–infected Ly5.1 donor mice on day 18 p.i. using an Aria IIIu sorter. Next, ∼80,000 cells of each respective subset were transferred into separate groups of infection-matched WT mice. The phenotypes of donor-derived cells were assessed in spleens 8 d following adoptive transfer.

scRNA-seq

A total of three mice were sacrificed on days 33 (M1), 33 (M2), and 35 (M3) post-infection with LCMV Clone 13. Three other mice were sacrificed on day 28 p.i., with cells later pooled to generate one biological replicate (M4). Spleens were harvested, processed into single-cell suspensions in FACS buffer, and CD8^{+}CD44^{+}GP33^{+} cells were sorted using a BD FACSAria flow sorter (BD Biosciences). Cells were then loaded into the 10× Chromium Controller (10× Genomics) for barcoding. scRNA-seq libraries of M1, M2, and M3 were prepared using the Chromium Single Cell 5′ v2 Reagent Kit according to the manufacturer's protocol. scRNA-seq libraries of M4 were prepared using the Chromium Single Cell 5′ v3 Reagent Kit according to the manufacturer's protocol. Aliquots of amplified cDNA were taken from each sample for scTCR-seq (see below). scRNA-seq libraries were quantified using a KAPA library quantification kit (Roche Sequencing). Samples M1, M2, and M3 were loaded onto an Illumina NextSeq 500 sequencer. A NextSeq 500/550 High Output Kit v2.5 (150 cycles; 20024907; Illumina) with 28 cycles for read 1, 91 cycles for read 2, and 8 cycles for i7 index reads was used for M1 and M2. A NextSeq 500/550 High Output Kit v2 (150 cycles; 20024907; Illumina) with 26 cycles for read 1, 98 cycles for read 2, and 8 cycles for i7 index reads was used for M3. Sample M4 was normalized to 1.2 nM and loaded onto an Illumina HiSeq 4000 flow cell and sequenced using 28 cycles for read 1, 98 cycles for read 2, and 8 cycles for i7 index reads. A positive control (prepared bacteriophage Phi X library) provided by Illumina was spiked into every lane at a concentration of

0.3% to monitor sequencing quality in real time. Raw sequencing data were downloaded from Illumina BaseSpace, then demultiplexed and converted to gene-barcode matrices using the "mkfastq" and "count" functions in Cell Ranger v3.0 (10× Genomics). 2,987, 2,567, 3,540, and 1,359 cells were recovered from samples M1, M2, M3, and M4, respectively.

scTCR-seq

A 10 µl aliquot of each sample's amplified cDNA was taken for scTCR-seq. The standard 10× protocol was followed for TCR gene amplification. Libraries were quantified using a KAPA library quantification kit (Roche Sequencing) and then loaded onto an Illumina NextSeq 500 sequencer using a NextSeq 500/550 High Output Kit v2.5 (300 cycles; 20024908; Illumina) or HiSeq 4000 flow cell with 150 cycles for read 1, 150 cycles for read 2, and 8 cycles for i7 index reads. Raw sequencing data were downloaded from Illumina BaseSpace, then demultiplexed and converted to gene-barcode matrices using the "mkfastq" and "vdj" functions in Cell Ranger v3.0 (10× Genomics). 7,017, 3736, 10921, and 3706 TCR reads were recovered from samples M1, M2, M3, and M4, respectively.

Data analysis

Analysis was primarily performed in R (v 3.6.1) using the package Seurat (v 3.1; Butler et al., 2018; Stuart et al., 2019), with the package tidyverse (v 1.2.1; Wickham et al., 2019) used to organize data and the package ggplot2 (v 3.2.1) used to generate figures. scRNA-seq data sets were integrated and then scTCR-seq data were added. scRNA-seq data were filtered to keep cells with a low percentage of mitochondrial genes in the transcriptome (<5%) and between 200 and 3,000 unique genes to exclude poor quality reads and doublets. Cell cycle scores were regressed when scaling gene expression values and TCR genes were regressed during the clustering process, which was performed with the Louvain algorithm within Seurat and visualized with UMAP. Cells other than CD8⁺ T cells, naive CD8⁺ T cells, sample-specific outliers, and cells not belonging to clones with at least two cells were excluded. A clone was defined as a group of cells sharing the same TCR α and β chain CDR3 nucleotide sequences. Sample M4 was excluded from analysis of clonal overlap among mice (Fig. S1) because it was a pooled sample but was used for all other analyses and figures. Trajectory analyses were performed using Monocle (v 2.12.0; Qiu et al., 2017). The Monocle tree structure was generated using the DDRTree algorithm with the top 75 differentially expressed genes from each Seurat cluster. Clonal diversity metrics were calculated using vegan (v 2.5.6). STARTRAC (v 0.1.0; Zhang et al., 2018) was used to calculate further clonal metrics of diversity and transitional potential. Chord diagrams were generated with circlize (v 0.4.8; Gu et al., 2014) and Venn diagrams with VennDiagram (v 1.6.20; Chen and Boutros, 2011).

TCR:pMHC models were generated as follows. Full TCR nucleotide sequences for clones with at least 10 cells were extracted from scTCR-seq data. ExPASy (Gasteiger et al., 2003) was used to translate nucleotide sequences to amino acid sequences. Each full TCR sequence was paired with the LCMV GP_{33-41} sequence (KAVYNFATC) and the mouse class I MHC H-$2D^b$ sequence and used as input to the TCRpMHCmodels webserver (Jensen et al., 2019). Structures generated with the webserver were then imported into Rosetta (v 3.8). Each structure was independently relaxed 100 times, with only the variants with the 10 lowest TCR:pMHC binding energies per structure selected for further use to exclude variants with early termination of relaxation due to energetic local minima. The ref2015 score function was used to calculate energies for all structures (Alford et al., 2017), with units given as Rosetta Energy Units. These 10 TCR:pMHC-binding energies per clone were averaged and multiplied by −1 to calculate the quantitative affinity for each clone. Quantitative avidity was calculated by multiplying quantitative affinity by the average number of normalized reads per cell of TCR constant chain genes (*Trac*, *Trbc1*, and *Trbc2*) as a metric of the relative number of TCRs expressed by each cell. For clonal calculations, values were averaged across all cells per clone.

Statistical analysis

Statistical tests for flow cytometry data were performed using Graphpad Prism 7. P values were calculated using either two-tailed unpaired Student's *t* tests or one-way ANOVA while correcting for multiple comparisons through the Tukey method. Linear regressions were performed using the ordinary least squares method in R (v 3.6.1). Boxplots and violin plots were compared pairwise in R using the Wilcoxon test with Holm-Sidak correction.

Online supplemental material

Fig. S1 shows kinetic data of the four major CD8⁺ T cell subsets and evidence indicating the existence of a fifth CD8⁺ T cell subset. Fig. S2 shows further pseudotime plots of antiviral CD8⁺ T cell differentiation, including when cells are clustered into five subsets rather than four. Fig. S3 shows further data related to IFN signaling, poly (I:C) stimulation, and *Irf7* knockout experiments. Fig. S4 shows plots of quantitative affinity and TCR characteristics. Fig. S5 shows *Ptpn6* (encodes SHP-1) expression and CD8 T cell subset distributions following *Ptpn6* genetic ablation.

Data and code availability

scRNA-seq and scTCR-seq data are available in the GEO database with the following accession numbers: GSE206230 (M1, M2, and M3; days 33, 33, and 35 p.i., respectively; scRNA-seq and scTCR-seq), GSM5530565 (M4, day 28 p.i.; scRNA-seq), and GSE210116 (M4, day 28 p.i., scTCR-seq). All other raw data and scripts are available from the corresponding author upon request.

Acknowledgments

We would like to thank Dr. Michael Wedemeyer and Dr. Acacia Dishman for their assistance with Rosetta and their commitment to promoting computational biology training at MCW. This research was completed in part with computational resources and technical support provided by the Research Computing Center at MCW.

This work is supported by National Insitute of Health grants AI125741 (W. Cui), AI148403 (W. Cui), AI066232 (S.M. Kaech),

CA206483 (S.M. Kaech), DK127526 (M.Y. Kasmani), AI153537 (R. Zander), and CA246920 (P. Topchyan); by an American Cancer Society Research Scholar Grant (W. Cui); and by an Advancing a Healthier Wisconsin Endowment Grant (W. Cui). R. Zander was supported by the Cancer Research Institute Irvington Fellowship during a portion of this study. H.K. Chung is a Damon Runyon Fellow supported by a Damon Runyon Cancer Research Foundation grant (DRG-2374-19). M.Y. Kasmani. and P. Topchyan are members of the Medical Scientist Training Program at the MCW, which is partially supported by a training grant from National Institute of General Medical Sciences (T32-GM080202).

Author contributions: M.Y. Kasmani, R. Zander, and W. Cui conceptualized and designed the study. M.Y. Kasmani, R. Zander, H.K. Chung, Y. Chen, A. Khatun, M. Damo, and P. Topchyan performed experiments. M.Y. Kasmani and R. Zander analyzed most of the data and wrote the manuscript. R. Burns provided assistance with data analysis. K.E. Johnson, D. Levashova, U.M. Lorenz, and V.L. Tarakanova provided helpful insight and *Ptpn6*$^{fl/fl}$ mice. M.Y. Kasmani, R. Zander, N.S. Joshi, S.M. Kaech, and W. Cui revised and edited the manuscript. S.M. Kaech and W. Cui supervised the study.

Disclosures: S.M. Kaech reported personal fees from EvolveImmune Therapeutics, Affini-T Therapeutics, Arvinas, Pfizer, and Barer Institute outside the submitted work. No other disclosures were reported.

Submitted: 18 April 2022
Revised: 17 June 2022
Accepted: 8 August 2022

References

Ahmadzadeh, M., L.A. Johnson, B. Heemskerk, J.R. Wunderlich, M.E. Dudley, D.E. White, and S.A. Rosenberg. 2009. Tumor antigen-specific CD8 T cells infiltrating the tumor express high levels of PD-1 and are functionally impaired. *Blood*. 114:1537–1544. https://doi.org/10.1182/blood-2008-12-195792

Alfei, F., K. Kanev, M. Hofmann, M. Wu, H.E. Ghoneim, P. Roelli, D.T. Utzschneider, M. von Hoesslin, J.G. Cullen, Y. Fan, et al. 2019. TOX reinforces the phenotype and longevity of exhausted T cells in chronic viral infection. *Nature*. 571:265–269. https://doi.org/10.1038/s41586-019-1326-9

Alford, R.F., A. Leaver-Fay, J.R. Jeliazkov, M.J. O'Meara, F.P. DiMaio, H. Park, M.V. Shapovalov, P.D. Renfrew, V.K. Mulligan, K. Kappel, et al. 2017. The Rosetta all-atom energy function for macromolecular modeling and design. *J. Chem. Theor. Comput.* 13:3031–3048. https://doi.org/10.1021/acs.jctc.7b00125

Allard, M., B. Couturaud, L. Carretero-Iglesia, M.N. Duong, J. Schmidt, G.C. Monnot, P. Romero, D.E. Speiser, M. Hebeisen, and N. Rufer. 2017. TCR-ligand dissociation rate is a robust and stable biomarker of CD8$^+$ T cell potency. *JCI Insight*. 2:e92570. https://doi.org/10.1172/jci.insight.92570

Barber, D.L., E.J. Wherry, D. Masopust, B. Zhu, J.P. Allison, A.H. Sharpe, G.J. Freeman, and R. Ahmed. 2006. Restoring function in exhausted CD8 T cells during chronic viral infection. *Nature*. 439:682–687. https://doi.org/10.1038/nature04444

Beltra, J.C., S. Manne, M.S. Abdel-Hakeem, M. Kurachi, J.R. Giles, Z. Chen, V. Casella, S.F. Ngiow, O. Khan, Y.J. Huang, et al. 2020. Developmental relationships of four exhausted CD8$^+$ T cell subsets reveals underlying transcriptional and epigenetic landscape control mechanisms. *Immunity*. 52:825–841.e8. https://doi.org/10.1016/j.immuni.2020.04.014

Blackburn, S.D., H. Shin, G.J. Freeman, and E.J. Wherry. 2008. Selective expansion of a subset of exhausted CD8 T cells by alphaPD-L1 blockade. *Proc. Natl. Acad. Sci. USA*. 105:15016–15021. https://doi.org/10.1073/pnas.0801497105

Borg, N.A., L.K. Ely, T. Beddoe, W.A. Macdonald, H.H. Reid, C.S. Clements, A.W. Purcell, L. Kjer-Nielsen, J.J. Miles, S.R. Burrows, et al. 2005. The CDR3 regions of an immunodominant T cell receptor dictate the "energetic landscape" of peptide-MHC recognition. *Nat. Immunol.* 6:171–180. https://doi.org/10.1038/ni1155

Brooks, D.G., M.J. Trifilo, K.H. Edelmann, L. Teyton, D.B. McGavern, and M.B. Oldstone. 2006. Interleukin-10 determines viral clearance or persistence in vivo. *Nat. Med.* 12:1301–1309. https://doi.org/10.1038/nm1492

Butler, A., P. Hoffman, P. Smibert, E. Papalexi, and R. Satija. 2018. Integrating single-cell transcriptomic data across different conditions, technologies, and species. *Nat. Biotechnol.* 36:411–420. https://doi.org/10.1038/nbt.4096

Chang, Y.M., A. Wieland, Z.R. Li, S.J. Im, D.J. McGuire, H.T. Kissick, R. Antia, and R. Ahmed. 2020. T cell receptor diversity and lineage relationship between virus-specific CD8 T cell subsets during chronic lymphocytic choriomeningitis virus infection. *J. Virol.* 94:e00935-20. https://doi.org/10.1128/JVI.00935-20

Chen, H., and P.C. Boutros. 2011. VennDiagram: A package for the generation of highly-customizable Venn and euler diagrams in R. *BMC Bioinf.* 12:35. https://doi.org/10.1186/1471-2105-12-35

Chen, Y., R.A. Zander, X. Wu, D.M. Schauder, M.Y. Kasmani, J. Shen, S. Zheng, R. Burns, E.J. Taparowsky, and W. Cui. 2021. BATF regulates progenitor to cytolytic effector CD8$^+$ T cell transition during chronic viral infection. *Nat. Immunol.* 22:996–1007. https://doi.org/10.1038/s41590-021-00965-7

Chen, Z., Z. Ji, S.F. Ngiow, S. Manne, Z. Cai, A.C. Huang, J. Johnson, R.P. Staupe, B. Bengsch, C. Xu, et al. 2019. TCF-1-Centered transcriptional network drives an effector versus exhausted CD8 T cell-fate decision. *Immunity*. 51:840–855.e5. https://doi.org/10.1016/j.immuni.2019.09.013

Conley, J.M., M.P. Gallagher, and L.J. Berg. 2016. T cells and gene regulation: The switching on and turning up of genes after T cell receptor stimulation in CD8 T cells. *Front. Immunol.* 7:76. https://doi.org/10.3389/fimmu.2016.00076

Cornberg, M., L.L. Kenney, A.T. Chen, S.N. Waggoner, S.-K. Kim, H.P. Dienes, R.M. Welsh, and L.K. Selin. 2013. Clonal exhaustion as a mechanism to protect against severe immunopathology and death from an overwhelming CD8 T cell response. *Front. Immunol.* 4:475. https://doi.org/10.3389/fimmu.2013.00475

Dähling, S., A.M. Mansilla, K. Knöpper, A. Grafen, D.T. Utzschneider, M. Ugur, P.G. Whitney, A. Bachem, P. Arampatzi, F. Imdahl, et al. 2022. Type 1 conventional dendritic cells maintain and guide the differentiation of precursors of exhausted T cells in distinct cellular niches. *Immunity*. 55:656–670.e8. https://doi.org/10.1016/j.immuni.2022.03.006

Dash, P., A.J. Fiore-Gartland, T. Hertz, G.C. Wang, S. Sharma, A. Souquette, J.C. Crawford, E.B. Clemens, T.H.O. Nguyen, K. Kedzierska, et al. 2017. Quantifiable predictive features define epitope-specific T cell receptor repertoires. *Nature*. 547:89–93. https://doi.org/10.1038/nature22383

Davis, M.M., and P.J. Bjorkman. 1988. T-cell antigen receptor genes and T-cell recognition. *Nature*. 334:395–402. https://doi.org/10.1038/334395a0

Day, C.L., D.E. Kaufmann, P. Kiepiela, J.A. Brown, E.S. Moodley, S. Reddy, E.W. Mackey, J.D. Miller, A.J. Leslie, C. DePierres, et al. 2006. PD-1 expression on HIV-specific T cells is associated with T-cell exhaustion and disease progression. *Nature*. 443:350–354. https://doi.org/10.1038/nature05115

Dominguez, C.X., R.A. Amezquita, T. Guan, H.D. Marshall, N.S. Joshi, S.H. Kleinstein, and S.M. Kaech. 2015. The transcription factors ZEB2 and T-bet cooperate to program cytotoxic T cell terminal differentiation in response to LCMV viral infection. *J. Exp. Med.* 212:2041–2056. https://doi.org/10.1084/jem.20150186

Elias, R., F. Yan, N. Singla, N. Levonyack, J. Formella, A. Christie, P. Kapur, A.I. Bowman, H.J. Hammers, R. Hannan, and J. Brugarolas. 2019. Immune-related adverse events are associated with improved outcomes in ICI-treated renal cell carcinoma patients. *J. Clin. Oncol.* 37:645-645. https://doi.org/10.1200/jco.2019.37.7_suppl.645

Elsaesser, H., K. Sauer, and D.G. Brooks. 2009. IL-21 is required to control chronic viral infection. *Science*. 324:1569–1572. https://doi.org/10.1126/science.1174182

Feinerman, O., J. Veiga, J.R. Dorfman, R.N. Germain, and G. Altan-Bonnet. 2008. Variability and robustness in T cell activation from regulated heterogeneity in protein levels. *Science*. 321:1081–1084. https://doi.org/10.1126/science.1158013

Field, A.K., A.A. Tytell, E. Piperno, G.P. Lampson, M.M. Nemes, and M.R. Hilleman. 1972. Poly I:C, an inducer of interferon and interference

against virus infections. *Medicine*. 51:169–174. https://doi.org/10.1097/00005792-197205000-00002

Fowler, C.C., L.I. Pao, J.N. Blattman, and P.D. Greenberg. 2010. SHP-1 in T Cells limits the production of CD8 effector cells without impacting the formation of long-lived central memory cells. *J. Immunol.* 185:3256–3267. https://doi.org/10.4049/jimmunol.1001362

Fröhlich, A., J. Kisielow, I. Schmitz, S. Freigang, A.T. Shamshiev, J. Weber, B.J. Marsland, A. Oxenius, and M. Kopf. 2009. IL-21R on T cells is critical for sustained functionality and control of chronic viral infection. *Science*. 324:1576–1580. https://doi.org/10.1126/science.1172815

Gasteiger, E., A. Gattiker, C. Hoogland, I. Ivanyi, R.D. Appel, and A. Bairoch. 2003. ExPASy: The proteomics server for in-depth protein knowledge and analysis. *Nucleic Acids Res.* 31:3784–3788. https://doi.org/10.1093/nar/gkg563

Gerlach, C., J.W. van Heijst, E. Swart, D. Sie, N. Armstrong, R.M. Kerkhoven, D. Zehn, M.J. Bevan, K. Schepers, and T.N. Schumacher. 2010. One naive T cell, multiple fates in CD8+ T cell differentiation. *J. Exp. Med.* 207:1235–1246. https://doi.org/10.1084/jem.20091175

Gu, Z., L. Gu, R. Eils, M. Schlesner, and B. Brors. 2014. Circlize implements and enhances circular visualization in R. *Bioinformatics*. 30:2811–2812. https://doi.org/10.1093/bioinformatics/btu393

He, R., S. Hou, C. Liu, A. Zhang, Q. Bai, M. Han, Y. Yang, G. Wei, T. Shen, X. Yang, et al. 2016. Follicular CXCR5-expressing CD8+ T cells curtail chronic viral infection. *Nature*. 537:412–428. https://doi.org/10.1038/nature19317

Hebeisen, M., L. Baitsch, D. Presotto, P. Baumgaertner, P. Romero, O. Michielin, D.E. Speiser, and N. Rufer. 2013. SHP-1 phosphatase activity counteracts increased T cell receptor affinity. *J. Clin. Invest.* 123:1044–1056. https://doi.org/10.1172/JCI65325

Honda, K., A. Takaoka, and T. Taniguchi. 2006. Type I interferon [corrected] gene induction by the interferon regulatory factor family of transcription factors. *Immunity*. 25:349–360. https://doi.org/10.1016/j.immuni.2006.08.009

Huang, Z., J. Zak, I. Pratumchai, N. Shaabani, V.F. Vartabedian, N. Nguyen, T. Wu, C. Xiao, and J.R. Teijaro. 2019. IL-27 promotes the expansion of self-renewing CD8+ T cells in persistent viral infection. *J. Exp. Med.* 216:1791–1808. https://doi.org/10.1084/jem.20190173

Hudson, W.H., J. Gensheimer, M. Hashimoto, A. Wieland, R.M. Valanparambil, P. Li, J.X. Lin, B.T. Konieczny, S.J. Im, G.J. Freeman, et al. 2019. Proliferating transitory T cells with an effector-like transcriptional signature emerge from PD-1+ stem-like CD8+ T cells during chronic infection. *Immunity*. 51:1043–1058.e4. https://doi.org/10.1016/j.immuni.2019.11.002

Im, S.J., M. Hashimoto, M.Y. Gerner, J. Lee, H.T. Kissick, M.C. Burger, Q. Shan, J.S. Hale, J. Lee, T.H. Nasti, et al. 2016. Defining CD8+ T cells that provide the proliferative burst after PD-1 therapy. *Nature*. 537:417–421. https://doi.org/10.1038/nature19330

Jensen, K.K., V. Rantos, E.C. Jappe, T.H. Olsen, M.C. Jespersen, V. Jurtz, L.E. Jessen, E. Lanzarotti, S. Mahajan, B. Peters, et al. 2019. TCRpMHCmodels: Structural modelling of TCR-pMHC class I complexes. *Sci. Rep.* 9:14530. https://doi.org/10.1038/s41598-019-50932-4

Jin, X., D.E. Bauer, S.E. Tuttleton, S. Lewin, A. Gettie, J. Blanchard, C.E. Irwin, J.T. Safrit, J. Mittler, L. Weinberger, et al. 1999. Dramatic rise in plasma viremia after CD8+ T cell depletion in simian immunodeficiency virus-infected macaques. *J. Exp. Med.* 189:991–998. https://doi.org/10.1084/jem.189.6.991

Johnston, R.J., L. Comps-Agrar, J. Hackney, X. Yu, M. Huseni, Y. Yang, S. Park, V. Javinal, H. Chiu, B. Irving, et al. 2014. The immunoreceptor TIGIT regulates antitumor and antiviral CD8+ T cell effector function. *Cancer Cell*. 26:923–937. https://doi.org/10.1016/j.ccell.2014.10.018

Kanev, K., M. Wu, A. Drews, P. Roelli, C. Wurmser, M. von Hösslin, and D. Zehn. 2019. Proliferation-competent Tcf1+ CD8 T cells in dysfunctional populations are CD4 T cell help independent. *Proc. Natl. Acad. Sci. USA*. 116:20070–20076. https://doi.org/10.1073/pnas.1902701116

Khan, O., J.R. Giles, S. McDonald, S. Manne, S.F. Ngiow, K.P. Patel, M.T. Werner, A.C. Huang, K.A. Alexander, J.E. Wu, et al. 2019. TOX transcriptionally and epigenetically programs CD8+ T cell exhaustion. *Nature*. 571:211–218. https://doi.org/10.1038/s41586-019-1325-x

Khatun, A., M.Y. Kasmani, R. Zander, D.M. Schauder, J.P. Snook, J. Shen, X. Wu, R. Burns, Y.-G. Chen, C.-W. Lin, et al. 2021. Single-cell lineage mapping of a diverse virus-specific naive CD4 T cell repertoire. *J. Exp. Med.* 218:e20200650. https://doi.org/10.1084/jem.20200650

King, C.G., S. Koehli, B. Hausmann, M. Schmaler, D. Zehn, and E. Palmer. 2012. T cell affinity regulates asymmetric division, effector cell differentiation, and tissue Pathology. *Immunity*. 37:709–720. https://doi.org/10.1016/j.immuni.2012.06.021

Leong, Y.A., Y. Chen, H.S. Ong, D. Wu, K. Man, C. Deleage, M. Minnich, B.J. Meckiff, Y. Wei, Z. Hou, et al. 2016. CXCR5+ follicular cytotoxic T cells control viral infection in B cell follicles. *Nat. Immunol.* 17:1187–1196. https://doi.org/10.1038/ni.3543

Li, W., M.J. Hofer, A.L. Noçon, P. Manders, and I.L. Campbell. 2013. Interferon regulatory factor 7 (IRF7) is required for the optimal initial control but not subsequent clearance of lymphocytic choriomeningitis virus infection in mice. *Virology*. 439:152–162. https://doi.org/10.1016/j.virol.2013.02.015

Lieber, M.R. 1991. Site-specific recombination in the immune system. *FASEB J.* 5:2934–2944. https://doi.org/10.1096/fasebj.5.14.1752360

Liu, X., Y. Wang, H. Lu, J. Li, X. Yan, M. Xiao, J. Hao, A. Alekseev, H. Khong, T. Chen, et al. 2019. Genome-wide analysis identifies NR4A1 as a key mediator of T cell dysfunction. *Nature*. 567:525–529. https://doi.org/10.1038/s41586-019-0979-8

Lorenz, U. 2009. SHP-1 and SHP-2 in T cells: Two phosphatases functioning at many levels. *Immunol. Rev.* 228:342–359. https://doi.org/10.1111/j.1600-065X.2008.00760.x

Man, K., S.S. Gabriel, Y. Liao, R. Gloury, S. Preston, D.C. Henstridge, M. Pellegrini, D. Zehn, F. Berberich-Siebelt, M.A. Febbraio, et al. 2017. Transcription factor IRF4 promotes CD8+ T cell exhaustion and limits the development of memory-like T cells during chronic infection. *Immunity*. 47:1129–1141.e5. https://doi.org/10.1016/j.immuni.2017.11.021

Martinez, G.J., R.M. Pereira, T. Äijö, E.Y. Kim, F. Marangoni, M.E. Pipkin, S. Togher, V. Heissmeyer, Y.C. Zhang, S. Crotty, et al. 2015. The transcription factor NFAT promotes exhaustion of activated CD8+ T cells. *Immunity*. 42:265–278. https://doi.org/10.1016/j.immuni.2015.01.006

McLane, L.M., M.S. Abdel-Hakeem, and E.J. Wherry. 2019. CD8 T cell exhaustion during chronic viral infection and cancer. *Annu. Rev. Immunol.* 37:457–495. https://doi.org/10.1146/annurev-immunol-041015-055318

Michot, J.M., C. Bigenwald, S. Champiat, M. Collins, F. Carbonnel, S. Postel-Vinay, A. Berdelou, A. Varga, R. Bahleda, A. Hollebecque, et al. 2016. Immune-related adverse events with immune checkpoint blockade: A comprehensive review. *Eur. J. Cancer*. 54:139–148. https://doi.org/10.1016/j.ejca.2015.11.016

Miller, B.C., D.R. Sen, R. Al Abosy, K. Bi, Y.V. Virkud, M.W. LaFleur, K.B. Yates, A. Lako, K. Felt, G.S. Naik, et al. 2019. Subsets of exhausted CD8+ T cells differentially mediate tumor control and respond to checkpoint blockade. *Nat. Immunol.* 20:326–336. https://doi.org/10.1038/s41590-019-0312-6

Moskophidis, D., F. Lechner, H. Pircher, and R.M. Zinkernagel. 1993. Virus persistence in acutely infected immunocompetent mice by exhaustion of antiviral cytotoxic effector T cells. *Nature*. 362:758–761. https://doi.org/10.1038/362758a0

Mueller, S.N., and R. Ahmed. 2009. High antigen levels are the cause of T cell exhaustion during chronic viral infection. *Proc. Natl. Acad. Sci. USA*. 106:8623–8628. https://doi.org/10.1073/pnas.0809818106

Ngoi, S.M., M.G. Tovey, and A.T. Vella. 2008. Targeting poly(I:C) to the TLR3-independent pathway boosts effector CD8 T cell differentiation through IFN-alpha/beta. *J. Immunol.* 181:7670–7680. https://doi.org/10.4049/jimmunol.181.11.7670

Okada, N., H. Kawazoe, K. Takechi, Y. Matsudate, R. Utsunomiya, Y. Zamami, M. Goda, M. Imanishi, M. Chuma, N. Hidaka, et al. 2019. Association between immune-related adverse events and clinical efficacy in patients with melanoma treated with nivolumab: A multicenter retrospective study. *Clin. Ther.* 41:59–67. https://doi.org/10.1016/j.clinthera.2018.11.004

Omilusik, K.D., J.A. Best, B. Yu, S. Goossens, A. Weidemann, J.V. Nguyen, E. Seuntjens, A. Stryjewska, C. Zweier, R. Roychoudhuri, et al. 2015. Transcriptional repressor ZEB2 promotes terminal differentiation of CD8+ effector and memory T cell populations during infection. *J. Exp. Med.* 212:2027–2039. https://doi.org/10.1084/jem.20150194

Ozga, A.J., F. Moalli, J. Abe, J. Swoger, J. Sharpe, D. Zehn, M. Kreutzfeldt, D. Merkler, J. Ripoll, and J.V. Stein. 2016. pMHC affinity controls duration of CD8+ T cell–DC interactions and imprints timing of effector differentiation versus expansion. *J. Exp. Med.* 213:2811–2829. https://doi.org/10.1084/jem.20160206

Paley, M.A., D.C. Kroy, P.M. Odorizzi, J.B. Johnnidis, D.V. Dolfi, B.E. Barnett, E.K. Bikoff, E.J. Robertson, G.M. Lauer, S.L. Reiner, and E.J. Wherry. 2012. Progenitor and terminal subsets of CD8+ T cells cooperate to contain chronic viral infection. *Science*. 338:1220–1225. https://doi.org/10.1126/science.1229620

Pani, G., K.D. Fischer, I. Mlinaric-Rascan, and K.A. Siminovitch. 1996. Signaling capacity of the T cell antigen receptor is negatively regulated by the PTP1C tyrosine phosphatase. *J. Exp. Med.* 184:839–852. https://doi.org/10.1084/jem.184.3.839

Pao, L.I., K.P. Lam, J.M. Henderson, J.L. Kutok, M. Alimzhanov, L. Nitschke, M.L. Thomas, B.G. Neel, and K. Rajewsky. 2007. B cell-specific deletion of protein-tyrosine phosphatase Shp1 promotes B-1a cell development and causes systemic autoimmunity. *Immunity*. 27:35–48. https://doi.org/10.1016/j.immuni.2007.04.016

Qiu, X., Q. Mao, Y. Tang, L. Wang, R. Chawla, H.A. Pliner, and C. Trapnell. 2017. Reversed graph embedding resolves complex single-cell trajectories. *Nat. Methods*. 14:979–982. https://doi.org/10.1038/nmeth.4402

Radziewicz, H., C.C. Ibegbu, M.L. Fernandez, K.A. Workowski, K. Obideen, M. Wehbi, H.L. Hanson, J.P. Steinberg, D. Masopust, E.J. Wherry, et al. 2007. Liver-infiltrating lymphocytes in chronic human hepatitis C virus infection display an exhausted phenotype with high levels of PD-1 and low levels of CD127 expression. *J. Virol.* 81:2545–2553. https://doi.org/10.1128/jvi.02021-06

Raju, S., Y. Xia, B. Daniel, K.E. Yost, E. Bradshaw, E. Tonc, D.J. Verbaro, K. Kometani, W.M. Yokoyama, T. Kurosaki, et al. 2021. Identification of a T-bet hi quiescent exhausted CD8 T cell subpopulation that can differentiate into TIM3 + CX3CR1 + effectors and memory-like cells. *J. Immunol.* 206:2924–2936. https://doi.org/10.4049/jimmunol.2001348

Richter, K., T. Brocker, and A. Oxenius. 2012. Antigen amount dictates CD8$^+$T-cell exhaustion during chronic viral infection irrespective of the type of antigen presenting cell. *Eur. J. Immunol.* 42:2290–2304. https://doi.org/10.1002/eji.201142275

Rome, K.S., S.J. Stein, M. Kurachi, J. Petrovic, G.W. Schwartz, E.A. Mack, S. Uljon, W.W. Wu, A.G. DeHart, S.E. McClory, et al. 2020. Trib1 regulates T cell differentiation during chronic infection by restraining the effector program. *J. Exp. Med.* 217:e20190888. https://doi.org/10.1084/jem.20190888

Sade-Feldman, M., K. Yizhak, S.L. Bjorgaard, J.P. Ray, C.G. de Boer, R.W. Jenkins, D.J. Lieb, J.H. Chen, D.T. Frederick, M. Barzily-Rokni, et al. 2018. Defining T cell states associated with response to checkpoint immunotherapy in melanoma. *Cell*. 175:998–1013.e20. https://doi.org/10.1016/j.cell.2018.10.038

Sandu, I., D. Cerletti, N. Oetiker, M. Borsa, F. Wagen, I. Spadafora, S.P.M. Welten, U. Stolz, A. Oxenius, and M. Claassen. 2020. Landscape of exhausted virus-specific CD8 T cells in chronic LCMV infection. *Cell Rep.* 32:108078. https://doi.org/10.1016/j.celrep.2020.108078

Sato, K., H. Akamatsu, E. Murakami, S. Sasaki, K. Kanai, A. Hayata, N. Tokudome, K. Akamatsu, Y. Koh, H. Ueda, et al. 2018. Correlation between immune-related adverse events and efficacy in non-small cell lung cancer treated with nivolumab. *Lung Cancer*. 115:71–74. https://doi.org/10.1016/j.lungcan.2017.11.019

Schmitz, J.E., M.J. Kuroda, S. Santra, V.G. Sasseville, M.A. Simon, M.A. Lifton, P. Racz, K. Tenner-Racz, M. Dalesandro, B.J. Scallon, et al. 1999. Control of viremia in simian immunodeficiency virus infection by CD8$^+$ lymphocytes. *Science*. 283:857–860. https://doi.org/10.1126/science.283.5403.857

Schober, K., F. Voit, S. Grassmann, T.R. Müller, J. Eggert, S. Jarosch, B. Weißbrich, P. Hoffmann, L. Borkner, E. Nio, et al. 2020. Reverse TCR repertoire evolution toward dominant low-affinity clones during chronic CMV infection. *Nat. Immunol.* 21:434–441. https://doi.org/10.1038/s41590-020-0628-2

Scott, A.C., F. Dündar, P. Zumbo, S.S. Chandran, C.A. Klebanoff, M. Shakiba, P. Trivedi, L. Menocal, H. Appleby, S. Camara, et al. 2019. TOX is a critical regulator of tumour-specific T cell differentiation. *Nature*. 571:270–274. https://doi.org/10.1038/s41586-019-1324-y

Seo, H., J. Chen, E. González-Avalos, D. Samaniego-Castruita, A. Das, Y.H. Wang, I.F. López-Moyado, R.O. Georges, W. Zhang, A. Onodera, et al. 2019. TOX and TOX2 transcription factors cooperate with NR4A transcription factors to impose CD8 + T cell exhaustion. *Proc. Natl. Acad. Sci. USA*. 116:12410–12415. https://doi.org/10.1073/pnas.1905675116

Sircar, P., K.L. Furr, L.A. Dorosh, and N.L. Letvin. 2010. Clonal repertoires of virus-specific CD8 + T lymphocytes are shared in mucosal and systemic compartments during chronic simian immunodeficiency virus infection in rhesus monkeys. *J. Immunol.* 185:2191–2199. https://doi.org/10.4049/jimmunol.1001340

Snell, L.M., T.L. McGaha, and D.G. Brooks. 2017. Type I interferon in chronic virus infection and cancer. *Trends Immunol.* 38:542–557. https://doi.org/10.1016/j.it.2017.05.005

Snook, J.P., A.J. Soedel, H.A. Ekiz, R.M. O'Connell, and M.A. Williams. 2020. Inhibition of SHP-1 expands the repertoire of antitumor t cells available to respond to immune checkpoint blockade. *Cancer Immunol. Res.* 8:506–517. https://doi.org/10.1158/2326-6066.CIR-19-0690

Speiser, D.E., D.T. Utzschneider, S.G. Oberle, C. Münz, P. Romero, and D. Zehn. 2014. T cell differentiation in chronic infection and cancer: Functional adaptation or exhaustion? *Nat. Rev. Immunol.* 14:768–774. https://doi.org/10.1038/nri3740

Štefanová, I., B. Hemmer, M. Vergelli, R. Martin, W.E. Biddison, and R.N. Germain. 2003. TCR ligand discrimination is enforced by competing ERK positive and SHP-1 negative feedback pathways. *Nat. Immunol.* 4:248–254. https://doi.org/10.1038/ni895

Stromnes, I.M., C. Fowler, C.C. Casamina, C.M. Georgopolos, M.S. McAfee, T.M. Schmitt, X. Tan, T.-D. Kim, I. Choi, J.N. Blattman, and P.D. Greenberg. 2012. Abrogation of src homology region 2 domain-containing phosphatase 1 in tumor-specific T cells improves efficacy of adoptive immunotherapy by enhancing the effector function and accumulation of short-lived effector T cells in vivo. *J. Immunol.* 189:1812–1825. https://doi.org/10.4049/jimmunol.1200552

Stuart, T., A. Butler, P. Hoffman, C. Hafemeister, E. Papalexi, W.M. Mauck, Y. Hao, M. Stoeckius, P. Smibert, and R. Satija. 2019. Comprehensive integration of single-cell data. *Cell*. 177:1888–1902.e21. https://doi.org/10.1016/j.cell.2019.05.031

Teijaro, J.R., C. Ng, A.M. Lee, B.M. Sullivan, K.C.F. Sheehan, M. Welch, R.D. Schreiber, J.C. de la Torre, and M.B. Oldstone. 2013. Persistent LCMV infection is controlled by blockade of type I interferon signaling. *Science*. 340:207–211. https://doi.org/10.1126/science.1235214

Tinoco, R., V. Alcalde, Y. Yang, K. Sauer, and E.I. Zuniga. 2009. Cell-intrinsic transforming growth factor-β signaling mediates virus-specific CD8$^+$ T cell deletion and viral persistence in vivo. *Immunity*. 31:145–157. https://doi.org/10.1016/j.immuni.2009.06.015

Trautmann, L., M. Rimbert, K. Echasserieau, X. Saulquin, B. Neveu, J. Dechanet, V. Cerundolo, and M. Bonneville. 2005. Selection of T Cell clones expressing high-affinity public TCRs within human cytomegalovirus-specific CD8 T cell responses. *J. Immunol.* 175:6123–6132. https://doi.org/10.4049/jimmunol.175.9.6123

Utzschneider, D.T., F. Alfei, P. Roelli, D. Barras, V. Chennupati, S. Darbre, M. Delorenzi, D.D. Pinschewer, and D. Zehn. 2016a. High antigen levels induce an exhausted phenotype in a chronic infection without impairing T cell expansion and survival. *J. Exp. Med.* 213:1819–1834. https://doi.org/10.1084/jem.20150598

Utzschneider, D.T., M. Charmoy, V. Chennupati, L. Pousse, D.P. Ferreira, S. Calderon-Copete, M. Danilo, F. Alfei, M. Hofmann, D. Wieland, et al. 2016b. T cell factor 1-expressing memory-like CD8$^+$ T cells sustain the immune response to chronic viral infections. *Immunity*. 45:415–427. https://doi.org/10.1016/j.immuni.2016.07.021

Utzschneider, D.T., A. Legat, S.A. Fuertes Marraco, L. Carrié, I. Luescher, D.E. Speiser, and D. Zehn. 2013. T cells maintain an exhausted phenotype after antigen withdrawal and population reexpansion. *Nat. Immunol.* 14:603–610. https://doi.org/10.1038/ni.2606

Wherry, E.J., J.N. Blattman, K. Murali-Krishna, R. van der Most, and R. Ahmed. 2003. Viral persistence alters CD8 T-cell immunodominance and tissue distribution and results in distinct stages of functional impairment. *J. Virol.* 77:4911–4927. https://doi.org/10.1128/jvi.77.8.4911-4927.2003

Wherry, E.J., S.J. Ha, S.M. Kaech, W.N. Haining, S. Sarkar, V. Kalia, S. Subramaniam, J.N. Blattman, D.L. Barber, and R. Ahmed. 2007. Molecular signature of CD8$^+$ T cell exhaustion during chronic viral infection. *Immunity*. 27:670–684. https://doi.org/10.1016/j.immuni.2007.09.006

Wickham, H., M. Averick, J. Bryan, W. Chang, L. McGowan, R. François, G. Grolemund, A. Hayes, L. Henry, J. Hester, et al. 2019. Welcome to the tidyverse. *J. Open Source Softw.* 4:1686. https://doi.org/10.21105/joss.01686

Wilson, E.B., D.H. Yamada, H. Elsaesser, J. Herskovitz, J. Deng, G. Cheng, B.J. Aronow, C.L. Karp, and D.G. Brooks. 2013. Blockade of chronic type I interferon signaling to control persistent LCMV infection. *Science*. 340:202–207. https://doi.org/10.1126/science.1235208

Wu, T., Y. Ji, E.A. Moseman, H.C. Xu, M. Manglani, M. Kirby, S.M. Anderson, R. Handon, E. Kenyon, A. Elkahloun, et al. 2016. The TCF1-Bcl6 axis counteracts type I interferon to repress exhaustion and maintain T cell stemness. *Sci. Immunol.* 1:eaai8593. https://doi.org/10.1126/sciimmunol.aai8593

Wu, W., Q. Zhou, T. Masubuchi, X. Shi, H. Li, X. Xu, M. Huang, L. Meng, X. He, H. Zhu, et al. 2020. Multiple signaling roles of CD3ε and its application in CAR-T cell therapy. *Cell*. 182:855–871.e23. https://doi.org/10.1016/j.cell.2020.07.018

Yan, Y., S. Cao, X. Liu, S.M. Harrington, W.E. Bindeman, A.A. Adjei, J S.Jang, J.Jen, Y.Li, P. Chanana, et al. 2018. CX3CR1 identifies PD-1 therapy–responsive CD8$^+$ T cells that withstand chemotherapy during cancer chemoimmunotherapy. *JCI Insight*. 3:e97828. https://doi.org/10.1172/jci.insight.97828

Yao, C., H.-W. Sun, N.E. Lacey, Y. Ji, E.A. Moseman, H.-Y. Shih, E.F. Heuston, M. Kirby, S. Anderson, J. Cheng, et al. 2019. Single-cell RNA-seq reveals TOX as a key regulator of CD8$^+$ T cell persistence in chronic infection. *Nat. Immunol.* 20:890–901. https://doi.org/10.1038/s41590-019-0403-4

Yee, C., P.A. Savage, P.P. Lee, M.M. Davis, and P.D. Greenberg. 1999. Isolation of high avidity melanoma-reactive CTL from heterogeneous populations using peptide-MHC tetramers. *J. Immunol.* 162:2227–2234

Yermanos, A., I. Sandu, A. Pedrioli, M. Borsa, F. Wagen, N. Oetiker, S.P.M. Welten, K. Pallmer, S.T. Reddy, and A. Oxenius. 2020. Profiling virus-specific Tcf1+ T cell repertoires during acute and chronic viral infection. *Front. Immunol.* 11:986. https://doi.org/10.3389/fimmu.2020.00986

Yi, J.S., M. Du, and A.J. Zajac. 2009. A vital role for interleukin-21 in the control of a chronic viral infection. *Science*. 324:1572–1576. https://doi.org/10.1126/science.1175194

Zahm, C.D., V.T. Colluru, and D.G. McNeel. 2017. Vaccination with high-affinity epitopes impairs antitumor efficacy by increasing PD-1 expression on CD8$^+$ T cells. *Cancer Immunol. Res.* 5:630–641. https://doi.org/10.1158/2326-6066.CIR-16-0374

Zajac, A.J., J.N. Blattman, K. Murali-Krishna, D.J. Sourdive, M. Suresh, J.D. Altman, and R. Ahmed. 1998. Viral immune evasion due to persistence of activated T cells without effector function. *J. Exp. Med.* 188:2205–2213. https://doi.org/10.1084/jem.188.12.2205

Zander, R., D. Schauder, G. Xin, C. Nguyen, X. Wu, A. Zajac, and W. Cui. 2019. CD4$^+$ T cell help is required for the formation of a cytolytic CD8$^+$ T cell subset that protects against chronic infection and cancer. *Immunity*. 51:1028–1042.e4. https://doi.org/10.1016/j.immuni.2019.10.009

Zhang, D.J., Q. Wang, J. Wei, G. Baimukanova, F. Buchholz, A.F. Stewart, X. Mao, and N. Killeen. 2005. Selective expression of the cre recombinase in late-stage thymocytes using the distal promoter of the Lck gene. *J. Immunol.* 174:6725–6731. https://doi.org/10.4049/jimmunol.174.11.6725

Zhang, L., X. Yu, L. Zheng, Y. Zhang, Y. Li, Q. Fang, R. Gao, B. Kang, Q. Zhang, J.Y. Huang, et al. 2018. Lineage tracking reveals dynamic relationships of T cells in colorectal cancer. *Nature*. 564:268–272. https://doi.org/10.1038/s41586-018-0694-x

Zhou, S., A.M. Cerny, K.A. Fitzgerald, E.A. Kurt-Jones, and R.W. Finberg. 2012. Role of interferon regulatory factor 7 in T cell responses during acute lymphocytic choriomeningitis virus infection. *J. Virol.* 86:11254–11265. https://doi.org/10.1128/jvi.00576-12

Supplemental material

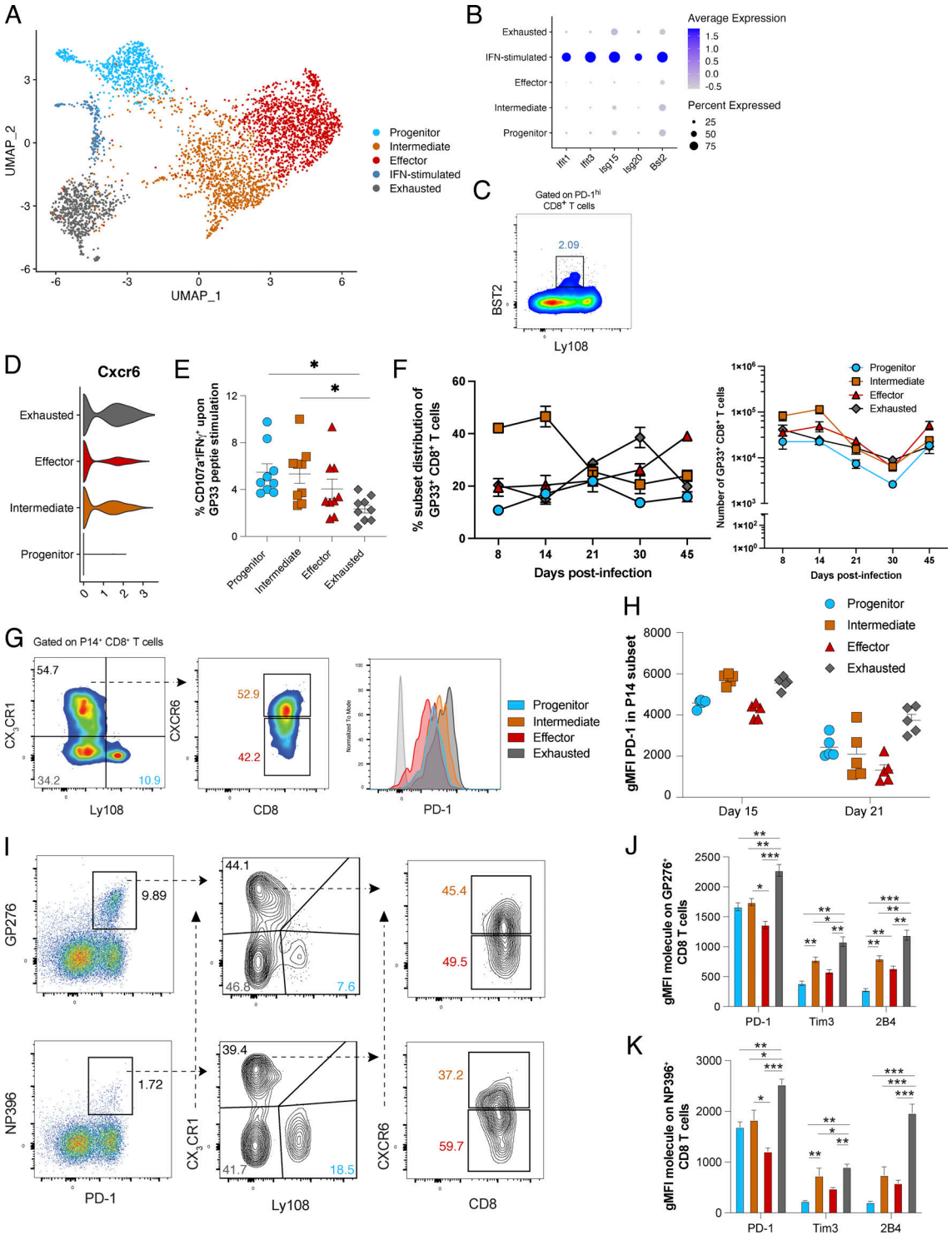

Figure S1. **Characterization of antigen-specific CD8⁺ T cell subsets in chronic viral infection.** Related to Fig. 2. **(A)** UMAP plot as in Fig. 2 A but with higher computational resolution to allow for visualization of five, rather than four, CD8⁺ T cell subsets. **(B)** Dot plot showing expression of genes stimulated by type I IFN signaling in CD8⁺ T cell scRNA-seq data. **(C)** Representative flow plot showing staining of the IFN-induced protein BST2 in antigen-experienced (PD-1^{hi}) CD8⁺ T cells. **(D)** Violin plot showing transcript expression of *Cxcr6*. **(E)** Frequency of CD107a⁺ IFNγ⁺ CD8⁺ T cells in each subset upon ex vivo stimulation with GP33 peptide. **(F)** Line graphs showing frequencies (left) and numbers (right) of GP33-specific CD8⁺ T cell subsets at different timepoints after LCMV Clone 13 infection. **(G and H)** Representative flow plots (G) and quantification of cell surface PD-1 MFI (H) in subsets of TCR transgenic P14 CD8⁺ T cells on days 15 and 21 p.i. **(I–K)** Representative flow plots (I) and inhibitory receptor MFI on subsets of GP276-specific (J) and NP396-specific (K) CD8⁺ T cells on day 21 after LCMV Clone 13 infection. Data (mean ± SEM) in E are from three mice per experiment and are pooled from three independent experiments. Data (mean ± SEM) in F are from six to nine mice per timepoint and are pooled from three independent experiments. Data (mean ± SEM) in H are from five P14 chimeric mice per timepoint and are representative of three independent experiments. Data (mean ± SEM) in J and K are from three mice per group and are representative of three independent experiments. * P < 0.05, ** P < 0.01, *** P < 0.001. gMFI, geometric MFI.

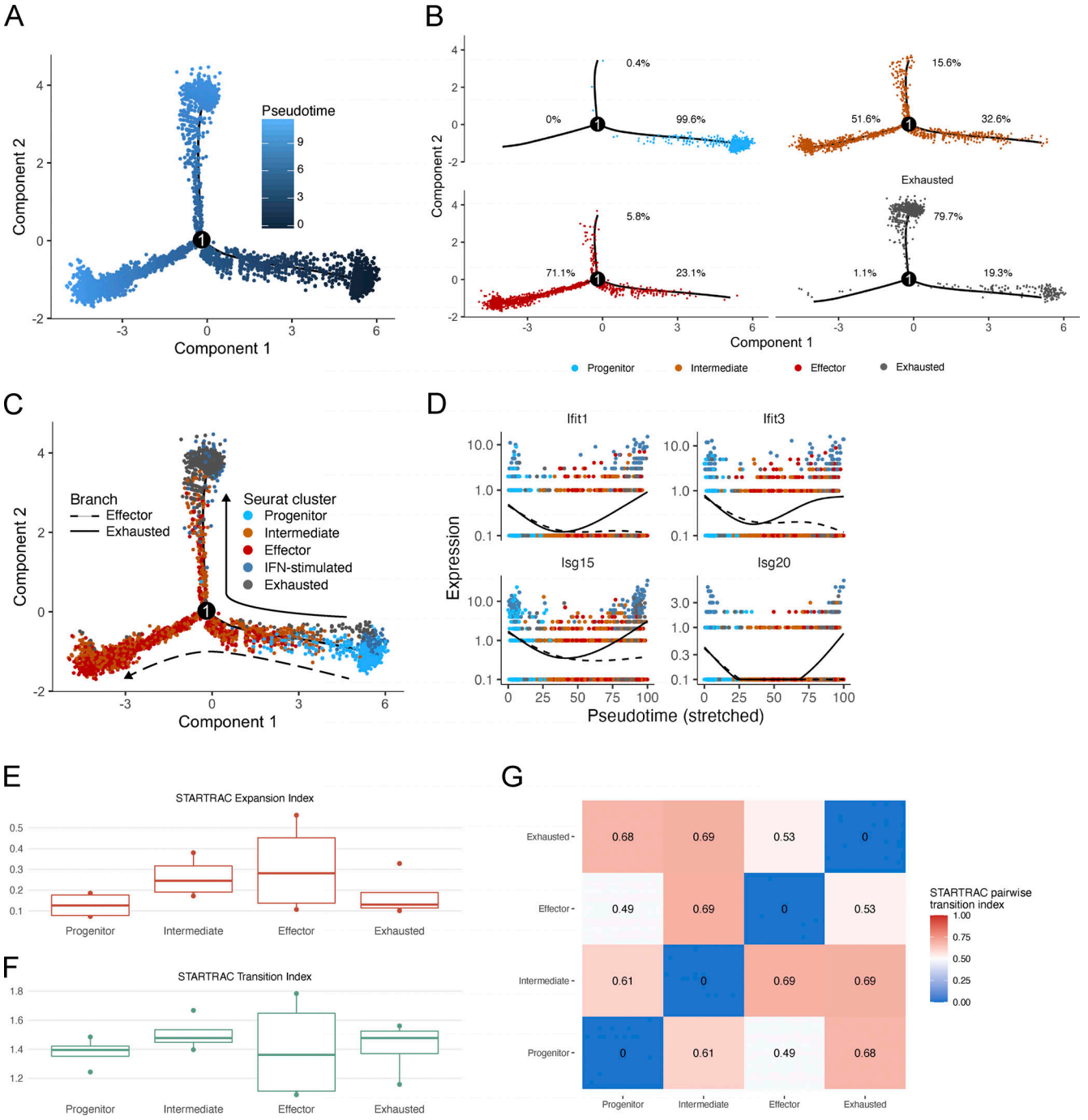

Figure S2. **Cellular and clonal trajectory analyses of CD8⁺ T cell subsets.** Related to Fig. 3. **(A)** Monocle tree trajectory as in Fig. 3 A but colored according to pseudotime. **(B)** Monocle tree trajectory as in Fig. 3 A but split by Seurat cluster for ease of viewing. Percentages show proportion of each Seurat phenotype spread among the three Monocle branches. **(C)** Monocle tree trajectory as in Fig. 3 A but colored by five, rather than four, CD8⁺ T cell subsets. **(D)** Monocle pseudotime expression of type I IFN–stimulated genes as in Fig. 3 D but colored by five Seurat subsets. **(E)** STARTRAC Expansion Index calculated on a clonal level and grouped by Seurat cluster. Higher scores indicate increased clonal expansion. **(F)** As in C but using the STARTRAC Transition Index. Higher scores indicate increased potential of phenotypic transition. **(G)** Pairwise STARTRAC Transition Index. Higher scores indicate increased potential of intercluster transition between the two clusters indicated.

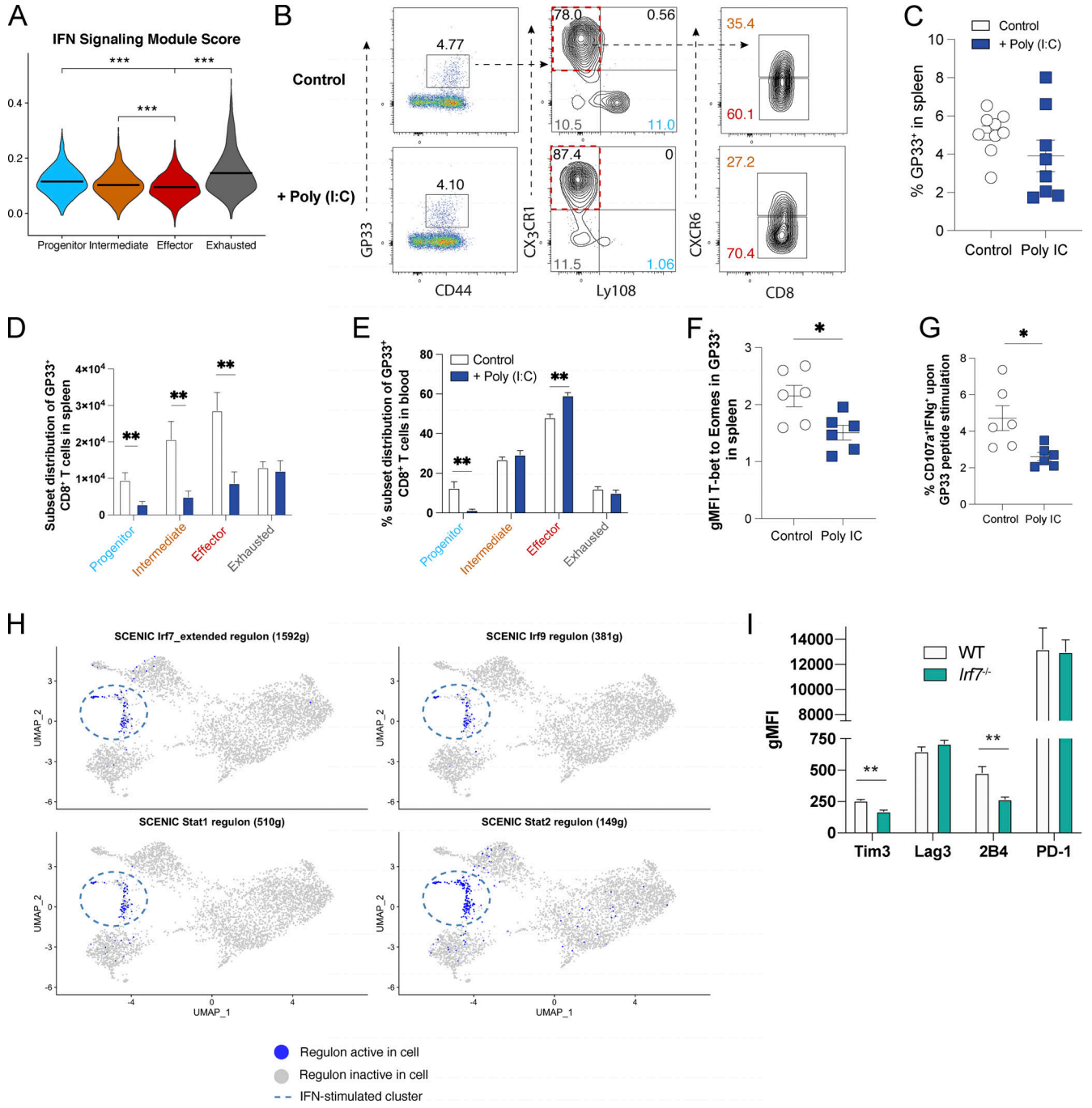

Figure S3. **Impact of type I IFN signaling and expression of the TF IRF7 on CD8⁺ T cell differentiation.** Related to Fig. 5. **(A)** Violin plot showing module scores of IFN signaling. **(B)** Representative flow plots of GP33⁺ CD44⁺ CD8⁺ T cell subsets collected from blood on day 24 p.i. with LCMV Clone 13. Mice were given either vehicle control (top) or Poly (I:C) (bottom). **(C)** Summary of frequency of GP33 antigen-specific CD8⁺ T cells in the spleens of control mice or mice given Poly (I:C). **(D)** Subset distribution of GP33 antigen-specific CD8⁺ T cells in the spleens of control mice or mice given Poly (I:C). **(E)** Subset distribution frequencies of GP33 antigen-specific CD8⁺ T cells in the blood of control mice or mice given Poly (I:C). **(F)** Summary of the ratio in MFI of T-bet to Eomes in GP33-specific CD8⁺ T cells from control and Poly (I:C)–treated mice. **(G)** Frequency of splenic CD107a⁺ IFNγ⁺ CD8⁺ T cells upon ex vivo stimulation with GP33 peptide. **(H)** Feature plots depicting SCENIC regulon activity of *Stat1*, *Stat2*, *Irf9*, and *Irf7* regulons in CD8⁺ T cell subsets. **(I)** Summary data showing the relative expression of co-inhibitory receptors on GP33⁺ CD8⁺ T cells from the spleens of WT mice or *Irf7*$^{-/-}$ mice. Data (mean ± SEM) in C–G are from three to four mice per group and are pooled from two independent experiments. Data (mean ± SEM) in I are from four mice per group and are representative of two independent experiments. * P < 0.05, ** P < 0.01, *** P < 0.001. gMFI, geometric MFI.

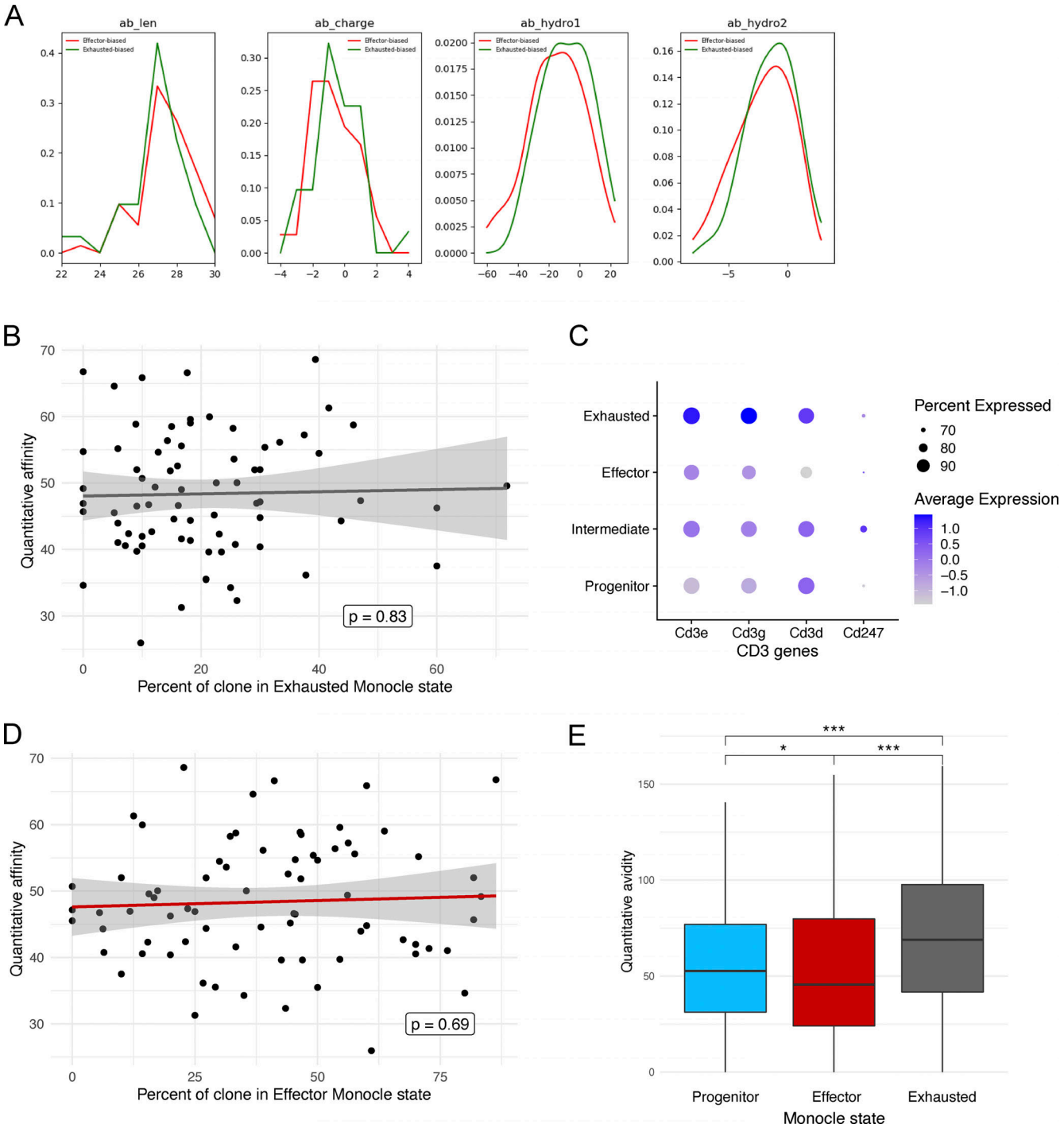

Figure S4. **TCR quantitative affinity and quantitative avidity.** Related to Fig. 7. **(A)** TCRdist analysis of CDR3 amino acid sequences of CD8 T cell clones. len, length; charge, amino acid charge; hydro, hydrophobicity. **(B)** Linear regression between quantitative affinity and percent of cells per clone in the exhausted Monocle state. Each point represents one clone. Gray shaded region, 95% confidence interval. **(C)** Dot plot showing expression of CD3 genes per cluster. Dot size, percent of cells expressing the gene; color, scaled expression. **(D)** As in B but with the percent of cells per clone in the effector Monocle state. **(E)** Box plot of quantitative avidity calculated on a per cell basis and grouped by Seurat cluster. Each box shows the lower quartile, median, and upper quartile. Whiskers span 1.5× interquartile range. * P < 0.05, *** P < 0.001.

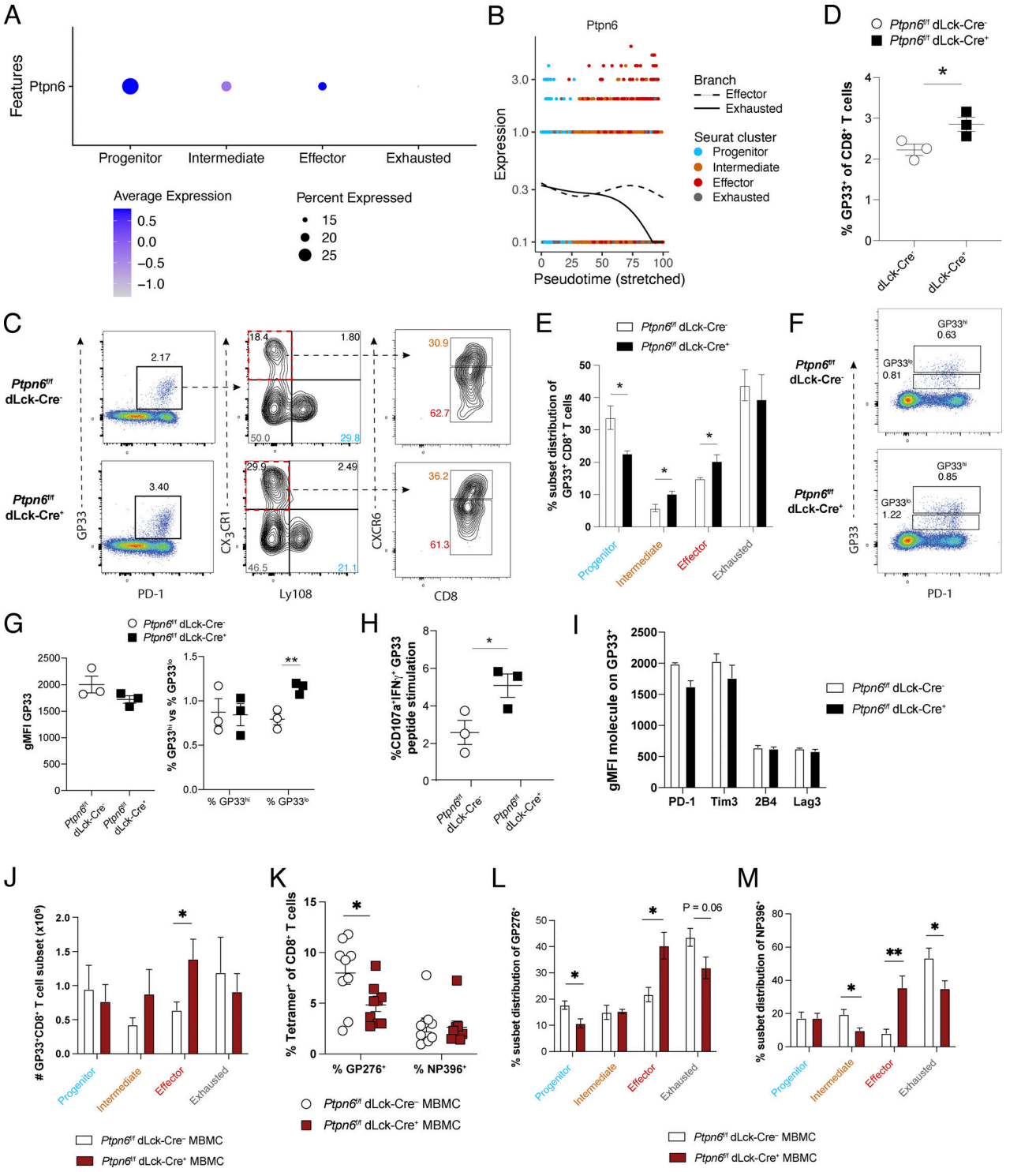

Figure S5. **SHP-1 expression and impact on CD8⁺ T cell fate decisions.** Related to Fig. 8. **(A)** Dot plot showing gene expression of *Ptpn6* (encodes SHP-1) among CD8⁺ T cell clusters. **(B)** Gene expression of *Ptpn6* over pseudotime. Dashed and solid lines denote transition from the progenitor to the effector or exhausted Monocle state, respectively. Colors denote the Seurat cluster identity of each cell. **(C)** Representative flow plots of splenic CD8⁺ T cells harvested from *Ptpn6*$^{flox/flox}$ dLck-Cre⁻ or *Ptpn6*$^{flox/flox}$ dLck-Cre⁺ mice 28 d p.i. with LCMV Clone 13. **(D)** Summary of frequency of GP33⁺ splenic CD8⁺ T cells in C. **(E)** Quantification of subset proportions from C. **(F)** Representative flow plots of splenic CD8⁺ T cells gated by GP33^{hi} and GP33^{lo} populations. **(G)** Summary of GP33 mean MFI (left) and frequency of GP33^{hi} and GP33^{lo} CD8⁺ T cells (right) in F. **(H)** Frequency of CD107a⁺ IFNγ⁺ CD8⁺ T cells upon ex vivo stimulation with GP33 peptide. **(I)** Summary of MFI of surface markers on GP33⁺ CD8⁺ T cells. **(J)** Summary of absolute numbers of GP33⁺ CD8⁺ T cell subsets. **(K)** Summary of frequency of GP276⁺ and NP396⁺ splenic CD8⁺ T cells. **(L)** Quantification of subset proportions of GP276⁺ splenic CD8⁺ T cells. **(M)** As in L, but with NP396⁺ splenic CD8⁺ T cells. Data (mean ± SEM) in D, E, and G–I are from three mice per group and are representative of two independent experiments. Data (mean ± SEM) in J–M are from five mice per group and are pooled from two independent experiments. One data point was excluded as its value was >2.5 SDs from the mean. * P < 0.05, ** P < 0.01. gMFI, geometric MFI.